https://doi.org/10.5194/egusphere-2024-488
Preprint. Discussion started: 28 February 2024

AERA-MIP: Emission pathways, remaining budgets and carbon cycle dynamics compatible with 1.5 ºC and 2 ºC global warming stabilization

Yona Silvy[1,2], Thomas L. Frölicher[1,2], Jens Terhaar[1,2,3], Fortunat Joos[1,2], Friedrich A. Burger[1,2], Fabrice Lacroix[1,2], Myles Allen[4,5], Raffaele Bernardello[6], Laurent Bopp[7], Victor Brovkin[8], Jonathan R. Buzan[1,2], Patricia Cadule[7], Martin Dix[9], John Dunne[10], Pierre Friedlingstein[7,11], Goran Georgievski[8], Tomohiro Hajima[12], Stuart Jenkins[4,5], Michio Kawamiya[12], Nancy Y. Kiang[13], Vladimir Lapin[6], Donghyun Lee[5], Paul Lerner[13,14], Nadine Mengis[15], Estela A. Monteiro[15], David Paynter[10], Glen P. Peters[16], Anastasia Romanou[13,14], Jörg Schwinger[17], Sarah Sparrow[18], Eric Stofferahn[10], Jerry Tjiputra[17], Etienne Tourigny[6], and Tilo Ziehn[9]

[1]Climate and Environmental Physics, Physics Institute, University of Bern, Switzerland
[2]Oeschger Centre for Climate Change Research, University of Bern, Switzerland
[3]Woods Hole Oceanographic Institution, Woods Hole, MA, USA
[4]Atmospheric, Oceanic and Planetary Physics, Department of Physics, University of Oxford, Oxford, UK
[5]Environmental Change Institute, School of Geography and the Environment, University of Oxford, Oxford, UK
[6]Barcelona Supercomputing Center, Barcelona, Spain
[7]LMD-IPSL, CNRS, Ecole normale supérieure / PSL, Sorbonne Université, Ecole Polytechnique, Paris, France
[8]Max Planck Institute for Meteorology, Hamburg, Germany
[9]CSIRO Environment, Aspendale, Australia
[10]NOAA/OAR Geophysical Fluid Dynamics Laboratory, Princeton, NJ, USA
[11]Faculty of Environment, Science and Economy, University of Exeter, Exeter, UK
[12]Japan Agency for Marine-Earth Science and Technology, Yokohama, Japan
[13]NASA Goddard Institute for Space Studies, New York, NY, USA
[14]Applied Physics and Applied Mathematics, Columbia University, New York, NY, USA
[15]GEOMAR Helmholtz Centre for Ocean Research Kiel, Kiel, Germany
[16]CICERO Center for International Climate Research, Oslo, Norway
[17]NORCE Norwegian Research Centre and Bjerknes Centre for Climate Research, Bergen, Norway
[18]Oxford e-Research Centre, Department of Engineering Science, University of Oxford, Oxford, UK

Correspondence: Yona Silvy (yona.silvy@unibe.ch)

Abstract. While international climate policies now focus on limiting global warming well below 2 °C, or pursuing 1.5 °C, the climate modeling community has not provided an experimental design in which all Earth System Models (ESMs) converge and stabilize at the same prescribed global warming levels. This gap hampers accurate estimations based on comprehensive ESMs of the carbon emission pathways needed to meet such agreed warming levels, and of the associated climate impacts under temperature stabilization. Here, we apply the Adaptive Emission Reduction Approach (AERA) with ESMs to provide such simulations in which all models converge at 1.5 °C and 2.0 °C warming levels by iteratively adjusting their emissions. These emission-driven simulations provide a wide range of emission pathways and resulting atmospheric CO_2 projections for a given warming level, uncovering uncertainty ranges that were previously missing in the traditional CMIP scenarios with prescribed

https://doi.org/10.5194/egusphere-2024-488
Preprint. Discussion started: 28 February 2024

greenhouse gas concentration pathways. Meeting the 1.5°C warming level necessitates a 40 % (model full range: 7 to 76 %) reduction in multi-model mean CO_2-forcing equivalent (CO_2-fe) emissions from 2025 to 2030, a 98 % (57 to 127 %) reduction from 2025 to 2050, and a stabilization at 1.0 (-1.7 to 2.9) PgC yr^{-1} from 2100 onward after the 1.5 °C target is reached. For the 2.0 °C warming level, CO_2-fe emissions require a 47 % (8 to 92 %) reduction until 2050 and a stabilization at 1.7 (-1.5 to 2.7) PgC yr^{-1} from 2100 onward. The on-average positive emissions under stabilized global temperatures are the result of a decreasing transient climate response to cumulative CO_2-fe emissions. This evolution is consistent with a slightly negative zero emissions commitment - initially assumed zero - and leads to an increase in the post-2025 CO_2-fe emission budget by a factor 2.2 (-0.8 to 6.9) by 2150 for the 1.5 °C warming level and a factor 1.4 (0.9 to 2.4) for the 2.0 °C warming level compared to its first estimate in 2025. Our simulations highlight shifts in carbon uptake dynamics under stabilized temperature, such as a cessation of the carbon sinks in the North Atlantic and in tropical forests. On the other hand, the Southern Ocean and the northern high-latitude land remain carbon sinks over centuries after temperatures stabilize. Overall, this new type of target-based emission-driven simulations offers a more coherent assessment across climate models and opens up a wide range of possibilities for studying both the carbon cycle and climate impacts, such as extreme events, under climate stabilization.

1 Introduction

Climate goals outlined in international policies, such as the 2015 Paris Agreement (UNFCCC, 2015), primarily focus on global warming targets. The Paris Agreement in particular aims to hold "the increase in the global average temperature to well below 2°C above pre-industrial levels" and to pursue efforts "to limit the temperature increase to 1.5°C above pre-industrial levels". Global warming levels are chosen in international policies as they are often directly correlated to global and regional impacts of climate change (IPCC, 2018; Seneviratne et al., 2016). Hence, each fraction of avoided warming reduces risks for humans and ecosystems (IPCC, 2022).

The Coupled Model Intercomparison Project (CMIP) provides climate projections of Earth System Models (ESM) for the 21th century and beyond. These projections, however, follow an approach that poses challenges in estimating carbon emission pathways and budgets that are consistent with the goals of the Paris Agreement. In CMIP projections, ESMs have traditionally been driven by prescribed pathways in the concentrations of CO_2 and other radiative agents (O'Neill et al., 2016; Meinshausen et al., 2020), although there is now a push towards more emission-driven scenario designs (Sanderson et al., 2023). For a given greenhouse gas emissions or concentrations trajectory, each ESM simulates different global warming trajectories (e.g., Tebaldi et al., 2021, and see schematic in Fig.1), primarily due to the wide range in climate sensitivity or in the transient climate response (e.g. Zelinka et al., 2020; Meehl et al., 2020; Arora et al., 2020). The varying responses of ESMs has lead to varying estimates for the cumulative CO_2 emissions until a given global warming level is reached (Rogelj et al., 2016; Tokarska et al., 2018). In addition, for the inverse problem, it is difficult to estimate the emission pathways that align with stabilizing the climate at specific global warming levels. Instead, the emission pathways and budgets for temperature stabilization were estimated with reduced-form models (Millar et al., 2017), Earth System Models of Intermediate Complexity (Steinacher et al., 2013; Matthews et al., 2017; Mengis and Matthews, 2020; Damon Matthews et al., 2021), or by the near-linear relationship

https://doi.org/10.5194/egusphere-2024-488
Preprint. Discussion started: 28 February 2024

between anthropogenic global surface warming and cumulative emissions suggested by ESMs (Allen et al., 2009; Matthews et al., 2009; Zickfeld et al., 2009).

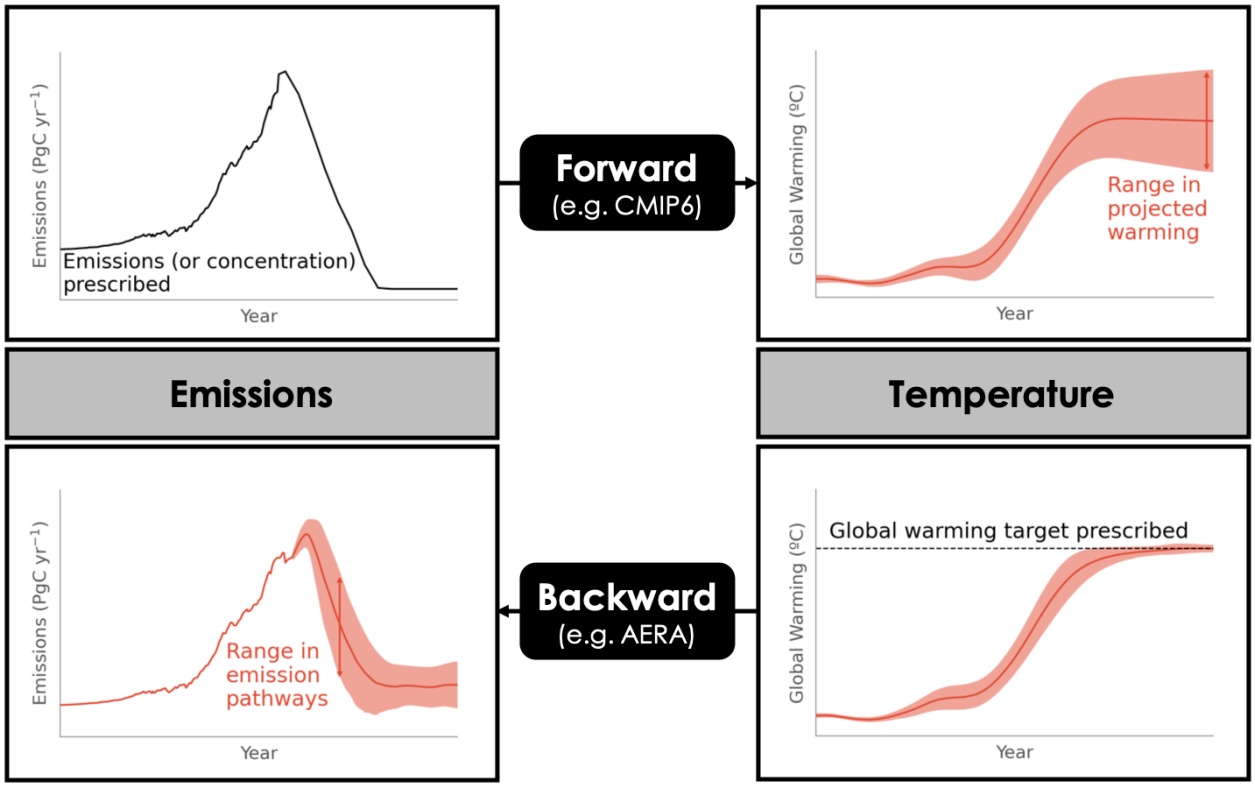

Figure 1. Schematic of the forward vs. backward modelling approach. Black lines indicate the same prescribed variable (emissions for CMIP, global warming target for AERA) in all models. Red lines indicate the resulting range across models in simulated temperature, and the resolved range in emissions in AERA.

Numerous studies have confirmed the near-linear response between global temperature increase and cumulative CO_2 emissions, with the slope of this relationship called the Transient Climate Response to Cumulative CO_2 emissions (TCRE). The TCRE has been estimated from observational data (e.g. Millar and Friedlingstein, 2018) and model experiments, and has been used to estimate the amount of cumulative emissions that could still be emitted before reaching a given global warming target (Meinshausen et al., 2009; Rogelj et al., 2016, 2019). The amount of cumulative CO_2 emissions up to the point of net zero CO_2 emissions is known as the remaining carbon budget (RCB) for a fixed warming level. The RCB from the beginning of year 2023, for example, has been estimated to be 250 $GtCO_2$ (68 PgC) for a 50 % chance of maintaining the global temperature below 1.5 ºC of warming, with its uncertainty range being 27 to 136 PgC, for an 83 %-17 % chance (Forster et al., 2023). For the 2.0 ºC target, the RCB ranges from 218 to 545 PgC. The uncertainty of the RCB is large due to uncertainties in the TCRE,

https://doi.org/10.5194/egusphere-2024-488
Preprint. Discussion started: 28 February 2024

climate-carbon feedbacks, climate response to zero emissions, unrepresented feedbacks, future warming from non-CO_2 agents (Rogelj et al., 2019), and pathway dependencies (Millar et al., 2017).

As the uncertainties in the TCRE, feedbacks, and future warming from non-CO_2 agents will unlikely be significantly reduced in the near future, an iterative and regular update of the RCB is necessary to ensure that the latest scientific understanding is included and to ensure policies can be judiciously implemented to avoid exceeding the given global warming levels. Through an adaptive process aligned with the "pledge and review" mechanism of the Paris Agreement, the RCB and emission pathways might be regularly updated at each stocktake period based on the best available science (Otto et al., 2015). The iterative approach ensures that the emission pathway remains in line with the warming target and adaptively adjusts to uncertainties in the evolution of the climate response, such as the potential warming or cooling at near-zero CO_2 emissions (Zero Emissions Commitment - ZEC - MacDougall et al., 2020), and the response to mitigation rates in non-CO_2 radiative agents. Such adaptive approaches have been proposed and tested with reduced complexity models running forward from present day, and offer promising potential. Goodwin et al. (2018a) introduced the "Adjusting Mitigation Pathways" method using a climate box model. However, limitations, including idealized emission trajectories, disregarding non-CO_2 agents in TCRE and RCB calculations, and challenges in reaching the target within the uncertainty range of $\pm$ 0.25 ºC by 2300, hinder its real-world applicability. Further approaches which do not make use of an adaptive RCB include backwards modelling approaches, like temperature tracking using models of intermediate complexity (EMICs; Matthews and Caldeira (2008); Zickfeld et al. (2009, 2013); Mengis et al. (2018)) or employing impulse-response functions with a simple climate model (Millar et al., 2017) to convert a smooth temperature trajectory into an emission pathway. In contrast, the recently developed Adaptive Emission Reduction Approach (AERA), validated with the Bern3D-LPX Earth System Model of Intermediate Complexity (Terhaar et al., 2022a, 2023), offers a less idealized approach and addresses several limitations inherent in previous approaches. AERA provides smoother emission pathways, incorporates non-CO_2 agents, always stabilizes at the warming targets within $\pm$0.2 °C, and can also be applied to run simulations that temporarily overshoot the warming target. However, as of now, AERA has not yet been implemented in comprehensive fully coupled ESMs.

Here, we implement the AERA introduced by Terhaar et al. (2022a) across a range of fully-coupled CO_2 emission-driven Earth System Models. This new Adaptive Emission Reduction Approach Model Intercomparison Project (AERA-MIP) provides projections that stabilize surface temperature to the same warming level. The AERA-MIP framework enables estimations of the remaining carbon budget, compatible emission pathways, and the ocean and land carbon cycle response to those pathways within scenarios of stabilized warming levels at 1.5 ºC or 2 ºC, which we present in this study. Other potential applications of AERA-MIP will be addressed in the Conclusions.

2 Methods

The detailed protocol for the simulations of the AERA-MIP is provided in Frölicher et al. (2022). The protocol is a slightly modified version from the method originally proposed by Terhaar et al. (2022a). The AERA code is distributed as a python

https://doi.org/10.5194/egusphere-2024-488
Preprint. Discussion started: 28 February 2024

module openly available under https://github.com/Jete90/AERA, with a guided documentation and examples. Below, the protocol is summarized before introducing the participating models, simulations, and carbon stock analysis.

2.1 Adaptive emission reduction approach - AERA

The goal of the AERA is to quantify successive future trajectories of CO_2-forcing equivalent (CO_2-fe) emissions that stabilize the global surface air temperature (GSAT) at a predetermined level (Terhaar et al., 2022a). The concept of CO_2-fe emissions is used to consider the emissions of various radiative forcing agents and precursors using a unified metric. CO_2-fe emissions of all non-CO_2 agents represent the quantity of CO_2 emissions that would cause the same radiative forcing trajectory as emissions from these non-CO_2 agents (Jenkins et al., 2018; Allen et al., 2018; Smith et al., 2021). Thus, the CO_2-fe metric is well suited for comparing emissions from different agents in the context of temperature stabilization pathways. AERA achieves the temperature stabilization at a predetermined warming level by estimating future CO_2-fe emissions based on the estimated TCRE-fe (the transient climate response to cumulative CO_2-fe emissions). The TCRE-fe in turn is derived from simulations of past annual GSAT, past fossil fuel and land-use change CO_2 emissions, and CO_2-fe emissions from non-CO_2 forcing agents calculated from their radiative forcing estimates (Jenkins et al., 2021).

The AERA consists of three steps, which are repeated every five years, mirroring the stocktaking mechanism implemented in the Paris Agreement (Terhaar et al., 2022a).

1. AERA estimates the anthropogenic warming ΔT from the simulated GSAT time series (relative to 1850-1900). The past anthropogenic warming is here estimated by applying a 31-year running mean with a linear extrapolation for the last 15 years, assuming constant warming rate based on the last 31 years. This is in contrast to the original AERA method, which employs an impulse response function on radiative forcing and temperature estimates to determine anthropogenic warming (Otto et al., 2015). The simple running mean method was applied here as it yields more robust results in cases where the model's radiative forcing is unknown (as is the case for most ESMs), and after reaching the temperature target.

2. The anthropogenic warming calculated in step 1 is then divided by the cumulative CO_2-fe emissions since 1850 to determine the TCRE-fe. Using this TCRE-fe metric, we compute the amount of CO_2-fe emissions that can still be emitted before reaching the target temperature. This remaining CO_2-fe emission budget, referred to as REB, is derived by dividing the remaining warming until the temperature target is reached ($\Delta T_{remaining}$) by the TCRE-fe value:

$$REB = \frac{\Delta T_{remaining}}{TCRE\text{-}fe} \tag{1}$$

3. The REB from step 2 is then distributed in the future using a cubic polynomial function. The parameters of the function are chosen to limit an overshoot in temperature and maintain minimal year-to-year changes in CO_2-fe emissions (see Terhaar et al. (2022a) for details). In contrast to Terhaar et al. (2022a) and to prevent large oscillations in the emissions in the ESMs when the warming levels are reached, we modified the minimum and maximum length (both now variable and depending on the REB and the annual emissions) of the cubic polynomial that distributes the CO_2-fe emissions over the future years.

https://doi.org/10.5194/egusphere-2024-488
Preprint. Discussion started: 28 February 2024

2.2 Earth System Models

Thirteen models have participated in the AERA-MIP: ten fully coupled Earth System Models (ACCESS-ESM1-5, CESM2, EC-Earth3-CC, NASA-GISS-E2-1-G-CC, GFDL-ESM2M, GFDL-ESM4, IPSL-CM6-LR-ESMCO2, MIROC-ES2L, MPI-ESM1-2-LR and NorESM2-LM), two models of intermediate complexity (Bern3D-LPX and UVic-ESCM-2.10), and one atmosphere-ocean general circulation model coupled to a carbon cycle emulator (HadCM3-FaIR2, see Appendix A for a description of the configuration). Nine of the fully-coupled ESMs have participated in the sixth phase of the coupled model intercomparison project (CMIP6), and GFDL-ESM2M has participated in CMIP5. Table A1 lists the models, their abbreviation used in this paper, as well as the corresponding references, the simulated time period and the number of ensemble members. A summary of their components has been already provided in several multi-ESM studies (e.g., Séférian et al., 2020; MacDougall et al., 2020; Arora et al., 2020; Canadell et al., 2021).

Small initial condition ensembles were provided by two participating ESMs to estimate the uncertainty associated with internal variability (Table A1). EC-Earth provided a three-member and GFDL-ESM2M a five-member ensemble. Ideally, larger ensemble simulations for every ESM would have been necessary to properly quantify the internal variability of each model (Lehner et al., 2020). However, even the small number of ensemble members available here provide a first-order estimate of internal variability.

ACCESS-ESM1-5 is the only model that does not converge to the target before 2200. The model most likely does not converge due to a strong mismatch between the estimate of non-CO_2 radiative forcing used in the AERA to estimate CO_2-fe emissions (from the RCP/SSP database, see below) and the non-CO_2 radiative forcing simulated in the model based on the prescribed atmospheric non-CO_2 radiative agents. Hence, results from ACCESS were excluded from subsequent multi-model statistics but are still shown for transparency in Fig. 2.

2.3 Simulations

The simulations of the AERA-MIP are performed until at least 2150 (except for HadCM3-FaIR2 until 2100) and up to 2300 to allow for enough time to reach the temperature target and stabilize global surface warming (Table A1). Simulations have been conducted for both the 1.5 °C and 2.0 °C temperature targets. To remove biases in simulated warming over the historical period relative to observations, we use the concept of a relative temperature target (Millar et al., 2017; Goodwin et al., 2018a; Terhaar et al., 2022a). Under this concept, the remaining allowable warming in 2020 is first estimated from observations. In a second step, the AERA adds this observation-based remaining allowable warming to the models' anthropogenic warming in 2020 to calculate the absolute temperature target in each model (see Frölicher et al., 2022). Thus, each model estimates the emission trajectory for the same remaining allowable warming in 2020, which is here estimated to be 0.28 ºC for the 1.5 ºC target and 0.78 °C for the 2.0 ºC target. These values were derived from the observation-based estimated warming of 1.22 °C in 2020 (Terhaar et al., 2022a).

All simulations branch off an emission-driven simulation (*esm-hist*) over the historical period following the CMIP6 protocol. After the end of the CMIP6 historical period in 2014, fossil fuel CO_2 emissions follow observed emissions until 2020

https://doi.org/10.5194/egusphere-2024-488
Preprint. Discussion started: 28 February 2024

(Friedlingstein et al., 2020; Le Quéré et al., 2021) and projected emissions from the Nationally Determined Contributions (NDCs; Climate Action Tracker: https://climateactiontracker.org/global/temperatures/, last accessed December 2021) from 2021 to 2025. Starting at the end of year 2025, fossil-fuel CO_2 emissions prescribed to the model are obtained every five years from AERA (see below and schematic in Fig. B1) by subtracting CO_2-fe emissions from prescribed non-CO_2 radiative agents and land use land cover change from the AERA-derived total CO_2-fe emission curve. Non-CO_2 agents as well as land use and land cover change are prescribed as in the SSP1-2.6 scenario after 2015. This low emission high mitigation scenario is often used in related climate stabilization approaches (e.g. Millar et al. (2017); Mengis et al. (2018)). An exception is the CMIP5-type GFDL-ESM2M which follows the CMIP5 protocol for the historical period as well as the RCP2.6 scenario instead of the SSP1-2.6 scenario for the non-CO_2 forcing agents and land use and land cover change. After 2100, no further changes occur in non-CO_2 forcing agents, land use and land cover. A schematic is provided in Fig. B1, summarising the feedback loop between the AERA module and the ESM during the post-2025 period of the simulations.

As the AERA calculates the CO_2-fe emissions, it requires information about emissions from non-CO_2 forcing agents ($E_{non\text{-}CO_2\text{-}fe}$) and CO_2 emissions from land use and land cover change (E_{LUC}; referred to as land use change emissions for simplicity from now on) to estimate the past TCRE-fe, on top of the past fossil fuel CO_2 emissions (E_{FOS}). Moreover, the future E_{FOS} prescribed to the model after each stocktake are calculated as the difference between the CO_2-fe emission curve ($E_{total\text{-}fe}$) from Step 3 of AERA, and the estimated future CO_2-fe emissions from land use change and non-CO_2 forcing agents:

$$E_{FOS} = E_{total\text{-}fe} - E_{LUC} - E_{non\text{-}CO_2\text{-}fe} \tag{2}$$

As most models do not directly output the radiative forcing of non-CO_2 agents (required to derive $E_{non\text{-}CO_2\text{-}fe}$), we estimate this time series from the radiative forcing given by the RCP/SSP database for both the historical period and SSP1-2.6 scenario. Some models, however, have provided an estimate of the simulated effective radiative forcing for all non-CO_2 radiative agents (see Table A2 and Fig. A1). For these models, the internally calculated effective radiative forcing estimates were used to derive the CO_2-fe emissions from the non-CO_2 forcing agents (Smith et al., 2021). Similarly, some models (see Table A2 and Fig. A2a) have conducted additional simulations to estimate E_{LUC} (Lawrence et al., 2016; Liddicoat et al., 2021). In that case, the model-specific E_{LUC} is prescribed to AERA instead of the default E_{LUC} estimate stemming from the Bern3D-LPX model that was scaled to align with the Global Carbon Budget estimates from 1850 to 2020. The default $E_{non\text{-}CO_2\text{-}fe}$ and E_{LUC} time series as well as the model-specific emissions for those who were able to estimate them are shown in Figs. A1 and A2a.

Although the future E_{LUC} and $E_{non\text{-}CO_2\text{-}fe}$ are prescribed in AERA to enable the extraction of future E_{FOS} as input to the models (Fig. B1), the future CO_2-fe emission curve $E_{total\text{-}fe}$ is largely insensitive to the chosen land use and non-CO_2 forcings (see tests in Terhaar et al. (2022a)).

Further details on the configuration of the AERA simulations in the models are provided in Appendix A.

https://doi.org/10.5194/egusphere-2024-488
Preprint. Discussion started: 28 February 2024

2.4 Remaining emission budget over time

While the TCRE is commonly considered approximately constant, recent studies suggest a potential variability in TCRE when CO_2 emissions are reduced, owing partly to a non-zero ZEC (Frölicher and Paynter, 2015; Steinacher and Joos, 2016; Nicholls et al., 2020; MacDougall et al., 2020). This indicates that the REB originally estimated at the end of 2025 may evolve over time, with the additional effect of potential non-linearities in the response of non-CO_2 forcing agents. To illustrate the temporal evolution of the REB from a fixed starting point, we reconstruct the CO_2-fe emission budget from beginning of year 2026 (EB_{2026}) at each stocktake by summing the REB calculated at the end of the stocktake year (t_{st}) and the already emitted CO_2-fe emissions between 2026 and that year:

$$EB_{2026}(t_{st}) = REB(t_{st}) + \int_{2026}^{t_{st}} E_{total\text{-}fe}(t)dt \tag{3}$$

$EB_{2026}(2025)$ is by definition $REB(2025)$.

2.5 Distribution of carbon in the Earth System

Within individual ESMs, all sources and sinks of the carbon mass balance are known and we can write:

$$E_{FOS} = G_{ATM} + S_{OCEAN} + (S_{LAND} - E_{LUC}) \tag{4}$$

E_{FOS} are the prescribed global fossil fuel CO_2 emissions during the historical period and calculated by AERA post 2025. G_{ATM} indicates the simulated atmospheric CO_2 growth rate in PgC yr^{-1} by using the conversion factor of 2.123 PgC ppm^{-1} (Enting et al., 1994). S_{OCEAN} is the net ocean carbon sink derived from the CO_2 flux into the ocean (CMIP6 variable *fgco2*). S_{LAND}-E_{LUC} denotes the net CO_2 flux into land and is derived from the net biosphere production (CMIP6 variable *nbp*). It includes the gross land carbon sink S_{LAND} minus emissions from land use and land cover change, E_{LUC}.

For the eight models that estimate their E_{LUC} term, we can quantify the gross land carbon sink S_{LAND} (Figure A2 and Appendix A), by adding the two diagnostics *nbp* + E_{LUC}. Thus, by rearranging Equation 4, we can separate net sources and sinks of CO_2:

$$E_{FOS} + E_{LUC} = G_{ATM} + S_{OCEAN} + S_{LAND} \tag{5}$$

As opposed to earlier studies (Liddicoat et al., 2021; Koven et al., 2022), atmospheric CO_2 is freely evolving and not prescribed, whereas E_{FOS} is prescribed and does not need to be diagnosed.

From Equation 5, we derive the cumulative airborne (CAF), ocean-borne fraction (COF) and land-borne fraction (CLF):

$$CAF = \frac{\int G_{ATM}}{\int (G_{ATM} + S_{OCEAN} + S_{LAND})} \tag{6}$$

$$COF = \frac{\int S_{OCEAN}}{\int (G_{ATM} + S_{OCEAN} + S_{LAND})} \tag{7}$$

https://doi.org/10.5194/egusphere-2024-488
Preprint. Discussion started: 28 February 2024

$$CLF = \frac{\int S_{LAND}}{\int (G_{ATM} + S_{OCEAN} + S_{LAND})} \quad (8)$$

with the $\int$ sign representing the time integral from 1850. Here we use $G_{ATM} + S_{OCEAN} + S_{LAND}$ instead of $E_{FOS} + E_{LUC}$ as the denominator of the cumulative fractions to avoid minor budget closure errors. These errors are negligible in most models, represent maximum a few percents (not shown), in which case they are very likely due to missing diagnostics.

3 Temperature, CO_2-fe emission and atmospheric CO_2 pathways

3.1 Convergence towards the temperature target

The AERA effectively stabilizes the simulated GSAT around the target warming level within an uncertainty of ±0.2 ºC (Fig. 2a,b). The uncertainty of ±0.2 ºC corresponds to the uncertainty with which anthropogenic warming can be determined from observations (Haustein et al., 2017; Jenkins et al., 2022a). Only the IPSL model temporarily leaves the 1.5 ºC uncertainty range and MIROC very shortly the 2.0 ºC uncertainty range. In the 1.5 ºC simulation (Fig. 2a), the multi-model mean GSAT anomaly (black thick line) enters the target temperature uncertainty range in 2026, i.e., the year the first AERA period begins. The temperature first peaks at 1.43 ºC in 2043 (min-max model range: 1.20 ºC to 1.57 ºC), temporarily drops to 1.40 ºC (1.23 ºC to 1.50 ºC) in 2069, and stabilizes around 1.44 ºC (1.25 ºC to 1.64 ºC) between 2100 and 2150. In the 2.0 ºC simulation (Fig. 2b), the multi-model mean GSAT anomaly enters the uncertainty envelope in 2061, and stabilizes at around 1.90 ºC (1.77 ºC to 2.09 ºC) between 2100 and 2150.

The convergence to the temperature target here shows that the AERA approach works for both intermediate complexity models, as shown previously (Terhaar et al., 2022a), as well as for fully-coupled ESMs. This is the case despite differences in E_{LUC} and $E_{non\text{-}CO_2\text{-}fe}$ prescribed to the AERA framework and in the models themselves. An exception is the ACCESS model that only converges to the respective targets by the late 22nd century after an overshoot of 0.3-0.5 °C (larger overshoot for the 1.5 °C target; see Methods for more details).

3.2 Compatible CO_2-fe emission pathways

For the 1.5 ºC warming target, CO_2-fe emissions decrease strongly and immediately after 2025 for all models, albeit with a large inter-model spread (Fig. 2c; Table 1). By 2030, CO_2-fe emissions drop to 8.1 (min-max range: 3.1 to 11.9) PgC yr^{-1}, a 40 % (7 % to 76 %) decline compared to 2025 levels of 13.7 (11.0 to 18.9) PgC yr^{-1}. During this strong decline phase, CO_2-fe emissions reach a maximum reduction of -2.0 (-0.4 to -3.6) PgC yr^{-2}. Afterwards, the emissions reach a temporary minimum at nearly zero in 2050 (0.2 PgC yr^{-1}; range: -3.6 to 5.0 PgC yr^{-1}), corresponding to a 98 % (57 % to 127 %) decline from 2025 levels, before peaking at 1.9 (-0.2 to 4.2) PgC yr^{-1} in 2077. This bounce in the CO_2-fe emission curve could be explained by the very rapid mitigation of non-CO_2 forcing agents in the early decades of the SSP1-2.6 scenario, causing slightly negative forcing-equivalent emissions approximately from 2030 to 2100 ($E_{non\text{-}CO_2\text{-}fe}$, see Fig. A1). Because this decline in $E_{non\text{-}CO_2\text{-}fe}$ is not

https://doi.org/10.5194/egusphere-2024-488
Preprint. Discussion started: 28 February 2024

accounted for in the first estimate of the REB at the end of year 2025, the emission budget is re-evaluated and increases in the stocktake years around 2050 relative to its 2025 estimate (Fig. 4a), leading to the on-average increase in emissions between 2050 and 2077. Subsequently, emissions decrease again to 1.0 (-1.7 to 2.9) PgC yr^{-1} between 2100 and 2150 when global mean temperatures have been stabilized. Until the end of the 22nd century, CO_2-fe emissions remain slightly positive on average. The positive emissions but large model spread during the temperature stabilization phase are consistent with the overall negative but highly uncertain multi-decade zero emissions commitment (i.e., global surface temperature change after setting CO_2 emissions to zero and keeping emissions at zero thereafter) highlighted by MacDougall et al. (2020) and Jenkins et al. (2022b) across a range of EMICs and ESMs. In 4 out of 13 models (GFDL-ESM4, IPSL, MPI, UVic), negative CO_2-fe emissions are not necessary to stabilize at the 1.5 °C warming level.

Achieving the 2.0 ºC target also requires strong CO_2-fe emission reductions, albeit less drastic than for the 1.5 ºC target. By 2030, multi-model mean CO_2-fe emissions decrease to 13.0 (10.9 to 17.1) PgC yr^{-1}, a 5.2 % (-1 % to 16 %) reduction from 2025 levels. By 2050, they further drop to 7.2 (1.3 to 11.4) PgC yr^{-1}, a 47 % (8 % to 92 %) decrease compared to 2025, and stabilize at 1.7 (range: -1.5 to 2.7) PgC yr^{-1} between 2100 and 2150. The maximum reduction rate between 2026 and 2100 is -0.7 (range: -2.3 to -0.1) PgC yr^{-2}. Only two models, EC-Earth and CESM2, exhibit temporary negative CO_2-fe emissions before 2150.

Several models simulate decadal-scale oscillations in emissions trajectories after reaching the temperature targets. These fluctuations partly stem from the challenge faced by AERA's anthropogenic warming estimation, utilizing an extended 31-year running mean, in distinguishing entirely between multi-decadal internal variability and anthropogenic trends in atmospheric temperature. In particular in NorESM2, large multi-decadal temperature variations due to Atlantic Meridional Overturning Circulation (AMOC) decline and subsequent recovery have been shown to occur when emissions are phased out (Schwinger et al., 2022). However, these oscillations lead to temperature fluctuations that remain within the $\pm$ 0.2°C range around the temperature target, except for a small undershoot simulated in the IPSL model, which takes a few decades to recover towards the warming target. This slow evolution of GSAT could be partly related to the large low-frequency internal variability exhibited in this model (Bonnet et al., 2021).

Beyond 2200, a time period for which only three models provide results, CO_2-fe emissions necessary for maintaining temperature stabilization are still projected to evolve slightly. For example, GFDL-ESM2M shows a slower reduction in CO_2-fe emissions during the 21st century compared to other models due to its low TCRE and a negative temperature response to zero emissions on decadal timescales. However, by the mid-22nd to 23rd century, CO_2-fe emissions in this model become slightly negative and will remain so for several centuries in response to a time-varying ZEC and continued warming in this model on multi-centennial timescales under zero emissions (Frölicher et al., 2014; Frölicher and Paynter, 2015). On the other hand, the Bern and MIROC models simulate continuous (albeit small) positive emissions on these timescales, reflecting continued cooling in these models under zero CO_2 emissions (negative ZEC) on multi-centennial timescales (MacDougall et al., 2020). This time dependency of the ZEC response following a period of CO_2 emissions erodes the value of the remaining budget concept as a fixed estimate beyond the first several decades around net zero.

https://doi.org/10.5194/egusphere-2024-488
Preprint. Discussion started: 28 February 2024

The simulated uncertainty range in CO_2-fe emission pathways across the models is not solely caused by model differences but also by internal variability (as diagnosed by the range across individual ensemble members of one model; Table 1, Figs. 3b and B2b). The internal variability uncertainty range diagnosed here represents a lower bound of the true internal variability uncertainty from ESMs as only a few ensemble members are available. Across the 3 ensemble members of EC-Earth and 5 ensemble members of GFDL-ESM2M, the min-max range in CO_2-fe emissions in 2050 is 3.9 PgC yr^{-1} for the 1.5 °C target and 0.7 PgC yr^{-1} for the 2.0 ºC target, corresponding to 45 % and 7 % of the multi-model range, respectively. These numbers rise to 66 % and 53 % between 2100 and 2150, respectively. The inter-member spread decreases during the temperature stabilization period. For example, in the 2.0 ºC target ensemble by GFDL-ESM2M, the inter-member range decreases from 2.7 PgC yr^{-1} in 2100-2150 to 1.1 PgC yr^{-1} in 2250-2300 (Fig. B2b). As for the maximum reduction rate in CO_2-fe emissions between 2026 and 2100, the GFDL-ESM2M ensemble members range from -1.3 to -0.1 PgC yr^{-2} for the 2.0 ºC target, corresponding to 56 % of the spread across all models.

https://doi.org/10.5194/egusphere-2024-488
Preprint. Discussion started: 28 February 2024

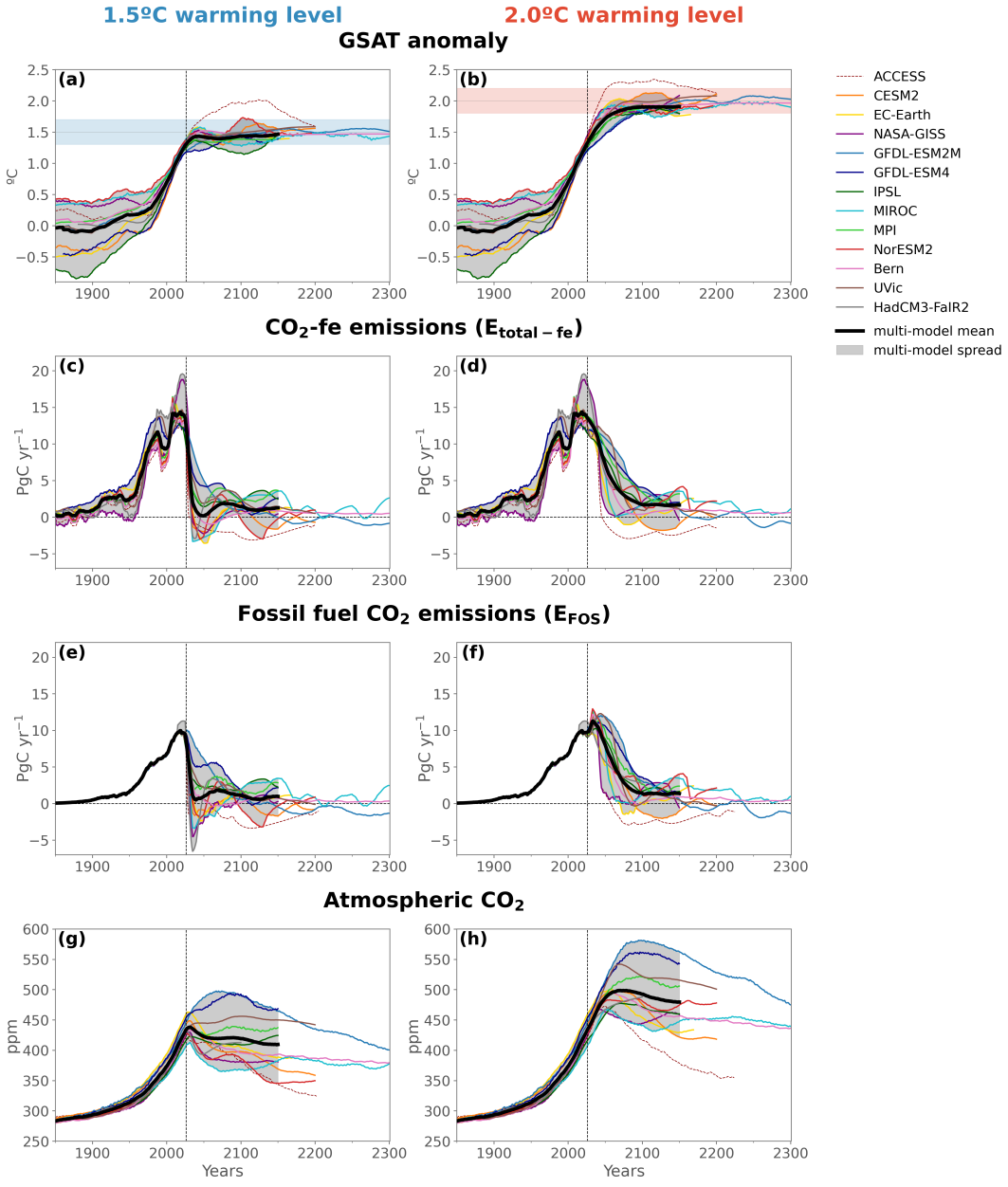

Figure 2. Simulated temperature anomaly, CO_2-fe emissions, fossil fuel CO_2 emissions and atmospheric CO_2 concentration for the 1.5ºC and 2.0ºC targets. Panels a) and b) display the 31-year running mean of the global surface air temperature (GSAT) anomaly, aligned with the observed value in 2020. Panels c) and d) illustrate CO_2-fe emissions and panels e) and f) show fossil fuel CO_2) emissions calculated by AERA. Panels g) and h) show the simulated atmospheric CO_2 mixing ratios. The multi-model mean, excluding the ACCESS model, is displayed by the black thick line, with the grey shading indicating the min-max spread. The ensemble mean is shown for models that have several ensemble members. The vertical dotted line at year 2026 marks the beginning of the AERA simulations.

https://doi.org/10.5194/egusphere-2024-488
Preprint. Discussion started: 28 February 2024

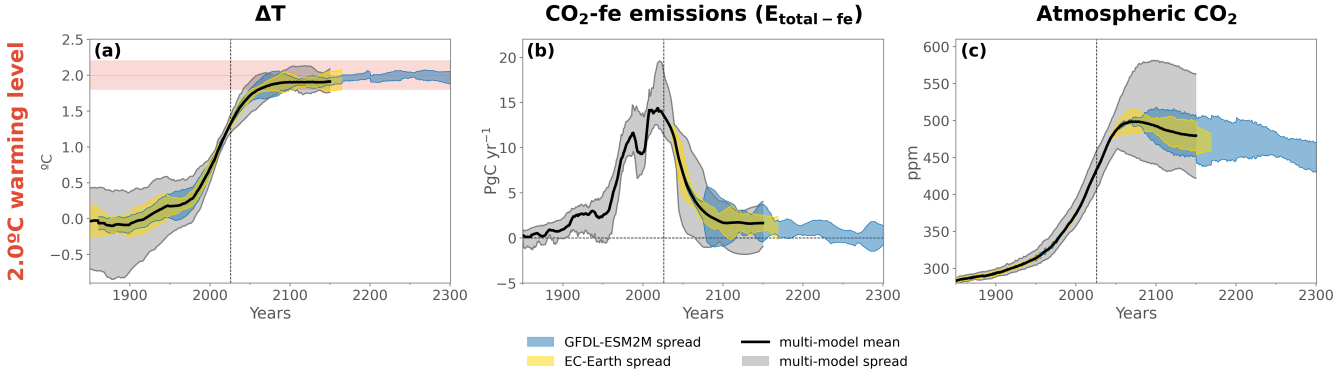

Figure 3. Comparison between model uncertainty and a lower bound for internal variability uncertainty in simulated temperature, CO_2-fe emissions and atmospheric CO_2 pathways for the 2.0 ºC target. Similar to Fig. 2b,d,h, but the panels show the multi-model min-max range in grey, and the inter-member min-max range of EC-Earth (3 members) in yellow and GFDL-ESM2M (5 members) in blue. The inter-member ensemble ranges are centered on the multi-model mean. For the 1.5 ºC target, refer to Fig. B2.

https://doi.org/10.5194/egusphere-2024-488
Preprint. Discussion started: 28 February 2024

Table 1. Simulated CO_2-fe emissions in 2025, 2030, 2050 and averaged between 2100-2150 in the 1.5 °C and 2.0 °C target simulations. The last column indicates the minimum of the derivative of the CO_2-fe curve, between 2026 and 2100. For models that performed several ensemble members, the ensemble mean is indicated, as well as the min-max range in the brackets.

Models	**CO_2-fe 2025 (PgC yr^{-1})**	**CO_2-fe 2030 (PgC yr^{-1})**		**CO_2-fe 2050 (PgC yr^{-1})**		**CO_2-fe 2100-2150 (PgC yr^{-1})**		**CO_2-fe max reduction between 2026 and 2100 (PgC yr^{-2})**	
		1.5 °C	**2.0 °C**	**1.5 °C**	**2.0 °C**	**1.5 °C**	**2.0 °C**	**1.5 °C**	**2.0 °C**
CESM2	13.2	9.2	12.9	-2.0	6.5	-0.5	-1.5	-3.2	-0.3
EC-Earth (3 members)	13.1	7.2 (4.3 ; 8.8)	11.8 (11.8 ; 11.8)	-3.6 (-4.8 ; -1.9)	3.8 (1.7 ; 7.0)	0.8 (-0.4 ; 1.4)	0.7 (0.1 ; 1.5)	-2.0 (-3.1 ; -1.2)	-0.8 (-0.8 ; -0.8)
NASA-GISS	18.1	11.9	17.1	-2.3	1.3	0.8	2.3	-3.6	-2.3
GFDL-ESM2M (5 members)	11.8	10.9 (10.8 ; 11.2)	12.0 (11.9 ; 12.0)	5.0 (3.5 ; 7.3)	10.8 (10.3 ; 11.0)	0.6 (-0.8 ; 2.6)	2.2 (1.2 ; 3.8)	-0.4 (-0.6 ; -0.2)	-0.5 (-1.3 ; -0.1)
GFDL-ESM4	11.8	9.3	11.8	4.2	9.6	1.4	2.7	-0.7	-0.1
IPSL (2 members)	11.0 (9.6 ; 12.4)	6.7 (5.7 ; 7.7)	10.9 (9.4 ; 12.4)	1.4 (0.6 ; 2.3)	8.0 (7.8 ; 8.3)	2.9 (2.8 ; 3.0)	2.1 (1.9 ; 2.2)	-0.9 (-1.0 ; -0.8)	-0.3 (-0.3 ; -0.3)
MIROC	12.2	8.4	13.1	-2.8	6.4	2.9	2.7	-3.5	-1.0
MPI	13.7	9.6	13.5	1.9	9.5	2.7	2.6	-1.4	-0.2
NorESM2	13.2	3.1	13.0	-2.6	7.0	-1.7	2.2	-2.2	-0.5
Bern (72 members)	12.9	7.3 (0.7 ; 11.5)	12.6 (12.0 ; 12.9)	-0.7 (-4.4 ; 5.3)	6.6 (-0.9 ; 10.6)	0.8 (-0.7 ; 2.5)	0.8 (-1.0 ; 2.8)	-1.7 (-3.2 ; -0.7)	-0.6 (-1.9 ; -0.1)
UVic	12.6	7.7	10.9	1.9	11.4	1.4	1.5	-1.1	-0.6
HadCM3-FaIR2 (29)	18.9 (12.1 ; 27.4)	6.1 (-3.6 ; 13.4)	16.2 (10.4 ; 25.2)	1.5 (-6.0 ; 7.1)	5.9 (-2.6 ; 9.8)	0.3 (-1.8 ; 2.0)	1.7 (-2.2 ; 4.9)	-3.5 (-6.2 ; -1.7)	-0.7 (-2.2 ; -0.3)
Mean (min;max)	**13.7 (11.0 ; 18.9**	**8.1 (3.1 ; 11.9)**	**13.0 (10.9 ; 17.1)**	**0.2 (-3.6 ; 5.0)**	**7.2 (1.3 ; 11.4)**	**1.0 (-1.7 ; 2.9)**	**1.7 (-1.5 ; 2.7)**	**-2.0 (-3.6 ; -0.4)**	**-0.7 (-2.3 ; -0.1)**

https://doi.org/10.5194/egusphere-2024-488
Preprint. Discussion started: 28 February 2024

3.3 Fossil fuel emissions

Fossil fuel emissions (E_{FOS}, see Equation 2) closely track the evolution of the CO_2-fe curve (Fig. 2e,f). In the 1.5 ºC scenario, the multi-model mean emissions remain slightly positive throughout the simulation, reaching a minimum in 2046 of 0.9 (-2.7 to 6.6) PgC yr^{-1}, peaking in 2069 at 1.7 (-1.0 to 5.4) PgC yr^{-1}, and gradually declining towards zero by the end of the 22nd century. Although the multi-model mean suggests that E_{FOS} can remain positive if emission reductions are fast and strong, negative emissions may still be necessary as five models simulate negative E_{FOS}, reaching -4.5 to -1.6 PgC yr^{-1} before 2050.

In the 2.0 ºC simulation, the multi-model mean reaches 8.2 (1.4 to 11.9) PgC yr^{-1} in 2050, stabilizes at 1.3 (-1.7 to 3.2) PgC yr^{-1} between 2100 and 2150, and slightly declines thereafter. In this scenario, only two models (CESM2 and EC-Earth) simulate non-negligible negative fossil fuel emissions before 2150, reaching -1.5 to -2.0 PgC yr^{-1}. A temporary increase in E_{FOS} occurs post 2025 in the 2.0 ºC simulation due to rapid reductions in non-CO_2 emissions ($E_{non\text{-}CO_2\text{-}fe}$) as prescribed in the SSP1-2.6 scenario (Fig. A1).

The uncertainty across models found here in residual emissions compatible with temperature stabilization appears to be in agreement with the results from Jenkins et al. (2022b), who diagnosed compatible emissions with halting warming after 1pctCO2 and 1.5ºC-compatible CO_2 emission-driven experiments. They calculate these emissions based on a theoretical framework (defining the RAZE parameter - rate of adjustment to zero emissions), results from the ZECMIP simulations, and a climate emulator. In their scenario in which non-CO_2 forcing agents follow SSP1-1.9 and CO_2 emissions linearly decrease to zero between 2021 and 2050, the best estimate of CO_2 emissions compatible with halting warming after 2050 is given at 0.66 PgC yr^{-1} (2.2 $GtCO_2$ yr^{-1}), with a 5th-95th percentile range of -2.2 to 1.9 PgC yr^{-1}. In their formulation of the multi-decade ZEC response, this equates to a small negative RAZE parameter whose uncertainty spans zero. On the other hand, Mengis et al. (2018) find that net negative fossil fuel CO_2 emissions are necessary to stabilize global surface temperature at 1.5 ºC in an observation-constrained carbon cycle perturbed-parameter ensemble of the UVic model. In their study, they used RCP2.6 non-CO_2 forcing extended to the year 2200, which in total causes positive radiative forcing between the first time the temperature is reached in 2055, and the period of stabilisation until 2200. They discuss that this is a likely cause for the net-negative CO_2 emissions.

3.4 Consequences for atmospheric CO_2

Since the simulations are CO_2 emission-driven, atmospheric CO_2 evolves dynamically (Fig. 2g,h). The multi-model mean atmospheric CO_2 reaches 420 ppm in 2020, slightly higher than the observed 412 ppm (Lan et al., 2023). In both temperature target simulations, the multi-model mean exhibits a peak and subsequent decline behavior. Atmospheric CO_2 peaks at 438 ppm in 2031 for the 1.5 ºC scenario and at 499 ppm in 2070 for the 2.0 ºC scenario, subsequently decreasing to 410 ppm in the 1.5 ºC scenario and to 480 ppm in the 2.0 ºC scenario by 2150. Thus, atmospheric CO_2 should start to decrease around 2030 to reach the 1.5 ºC target, according to the multi-model mean. Some models do not simulate such a smooth peak and decline behavior, and simulate in addition a (temporary) rise in atmospheric CO_2 due to a temporary rise in CO_2 emissions during or after the decline.

https://doi.org/10.5194/egusphere-2024-488
Preprint. Discussion started: 28 February 2024

The different CO_2 emissions and the strength of the land and ocean carbon sinks lead to large differences in atmospheric CO_2. The model min-max range in atmospheric CO_2 of 53 ppm in 2025 originates from different ocean and land carbon sinks and E_{LUC} emissions during the historical period (Hoffman et al., 2014) as all models have identical prescribed E_{FOS} (Fig. 2e; note HadCM3-FaIR2 differs due to the emissions being diagnosed and not prescribed, see Appendix A). After 2025, the spread in atmospheric CO_2 is also driven by the divergent E_{FOS} pathways and thus strongly increases, as E_{FOS} evolves also with the model-dependent AERA calculation every five years. The model min-max range expands to 105 ppm (1.5 ºC simulation) and 55 ppm (2.0 ºC) by 2050, 125 ppm (1.5 ºC) and 139 ppm (2.0 ºC) by 2100, and 123 ppm (1.5 ºC) and 141 ppm (2.0 ºC) by 2150.

Part of these large uncertainties may stem from internal variability (Fig. 3c and B2c). GFDL-ESM2M's 5 ensemble members show a min-max range of 54 ppm (1.5 ºC) and 49 ppm (2.0 ºC) by 2100, approximately 43 % and 40 %, respectively, of the multi-model range. EC-Earth's 3 ensemble members represent 29 % and 27 % of the model range in 2100. GFDL-ESM2M's range tends to decrease over the 23rd century, reaching 24 ppm (1.5 ºC) and 41 ppm (2.0 ºC) by 2300. Sensitivity simulations with the Bern model, covering the IPCC AR6 likely range of TCRE, exhibit an inter-member spread in atmospheric CO_2 levels that is as large as the inter-model spread, persisting during stabilization (not shown). Thus, while internal variability certainly plays an important role by 2100, differences in TCRE among the models remain the primary driver for the substantial model uncertainties in simulated atmospheric CO_2. Additional processes may be at play in explaining the model spread, not explained by differences in TCRE, such as the sensitivity to evolving non-CO_2 agents and the representation of land use land cover changes in the models. For example, the MIROC model has a low TCRE and negative ZEC (MacDougall et al., 2020), and yet it exhibits the lowest levels of atmospheric CO_2 already at the end of the historical period (Fig. 2g,h).

4 The evolving remaining emission budget

AERA calculates the simulated remaining CO_2-fe emission budget (REB) every five years based on the remaining allowable warming and the TCRE-fe relationship (see Equation 1 in Methods). At the beginning of year 2026, the start of the AERA period, the multi-model mean REB is 99 (47 to 204) PgC for the 1.5 ºC target and 409 (248 to 581) PgC for the 2.0 ºC target (Table 2). These REBs translate to 7 (3 to 14) years of CO_2-fe emissions sustained at mean 2020 levels (14.1 PgC yr^{-1}) for the 1.5 ºC target and 29 (18 to 41) years for the 2.0 ºC target before reaching the respective temperature target. Based on the model distribution, the REB from the beginning of year 2026 for a 50 % chance of staying below 1.5 ºC is 93 PgC and for staying below 2.0 ºC is 412 PgC. For a 66 % chance, the REB decreases to 84 PgC for the 1.5 ºC target and to 372 PgC for the 2.0 ºC target.

To compare these model-based estimates to other REB estimates from beginning of year 2021, we combine the CO_2-fe cumulative emissions of 70 PgC on average from 2021 to 2025 with the REB from beginning of year 2026, which yields a mean REB of 169 (113 to 264) PgC from the start of 2021 for the 1.5 ºC target and 479 (309 to 640) PgC for the 2.0 ºC target. Our model-estimated REB range encompasses the AERA-based REB calculations from observations of 167 PgC for 1.5 ºC and 472 PgC for 2.0 ºC (Terhaar et al., 2022a). The model's estimated REB also aligns with observation-constrained estimates

https://doi.org/10.5194/egusphere-2024-488
Preprint. Discussion started: 28 February 2024

by Jenkins et al. (2021) of 128-237 PgC for an 83 %-17 % probability of limiting warming to 1.5 ºC (also based on total CO_2-fe emissions).

Table 2. Remaining CO_2-fe Emission Budget (REB) from beginning of year 2026, calculated at the first stocktake (end of year 2025; $EB_{2026}(2025)$), and recalculated and averaged between 2100 and 2150, taking into account the emissions actually seen by the models since 2026 ($EB_{2026}(2100\text{-}2150)$; see Eq. 3).

Models	**REB at first stocktake $EB_{2026}(2025)$ (PgC)**		**EB_{2026} averaged between stocktakes 2100-2150 $EB_{2026}(2100\text{-}2150)$ (PgC)**	
	1.5 ºC	**2.0 ºC**	**1.5 ºC**	**2.0 ºC**
CESM2	100	345	6	298
EC-Earth	81	339	78	310
(3 members)	(52 ; 97)	(322 ; 359)	(16 ; 142)	(230 ; 365)
NASA-GISS	132	470	112	444
GFDL-ESM2M	204	581	353	778
(5 members)	(178 ; 244)	(534 ; 615)	(260 ; 423)	(678 ; 889)
GFDL-ESM4	111	407	475	756
IPSL	60	248	412	585
(2 members)	(58 ; 62)	(240 ; 256)	(386 ; 438)	(561 ; 609)
MIROC	86	478	259	599
MPI	104	416	416	721
NorESM2	47	442	-40	677
Bern	86	374	118	418
(72 members)	(24 ; 174)	(236 ; 554)	(-133 ; 396)	(109 ; 792)
UVic-ESCM	120	439	284	549
HadCM3-FaIR2	58	369	133	491
(29 members)	(-12 ; 148)	(230 ; 606)	(-89 ; 276)	(242 ; 718)
17^{th}, 33^{rd}, 50^{th}, 67^{th}, 83^{rd} percentiles	60, 84, 93, 106, 121	344, 372, 412, 440, 471	69, 116, 196, 302, 413	404, 474, 567, 619, 725
Mean (min;max)	**99 (47 ; 204)**	**409 (248 ; 581)**	**217 (-40 ; 475)**	**552 (297 ; 778)**

As the TCRE-fe evolves over time (see Fig. B3), so does the REB (Fig. 4), by definition (the two time series are almost perfectly anti-correlated). In our simulations, the multi-model mean REB as estimated at the beginning of year 2026 (EB_{2026}) is smaller than the emissions that are actually emitted until temperature stabilization. Or in other words, the actual EB is larger than the REB estimated at the beginning of 2026 (Table 2). Between 2100 and 2150, the multi-model mean estimate of EB_{2026} (calculated as the sum of the REB in the respective year and the already emitted emissions between 2026 and that year, see Methods for details) reaches 217 (-40 to 475) PgC for 1.5 ºC and 552 (297 to 778) PgC for 2.0 ºC. These updated emission

https://doi.org/10.5194/egusphere-2024-488
Preprint. Discussion started: 28 February 2024

budgets correspond to 15 years (-3 to 34) of sustained mean CO_2-fe emissions at 2020 levels for 1.5 ºC and 39 years (21 to 55) for 2.0 ºC. Based on the model distribution, this results in a remaining emission budget from beginning of 2026 of 116 PgC (474 PgC) for a 66 % chance of staying below 1.5 ºC (2.0 ºC). Thus, the simulated remaining emissions until temperature stabilization are 2.2 times larger than estimated at the beginning of 2026 for the 1.5 ºC target and 1.4 times larger for 2.0 ºC. This increase in the EB_{2026} between the beginning of the AERA period and the end of the simulations corresponds to a decrease in the TCRE-fe (Fig. B3), which is qualitatively consistent with a slightly negative multi-decade zero emissions commitment (and RAZE parameter) (MacDougall et al., 2020; Jenkins et al., 2022b) and the resulting residual positive emissions found on average across models during the stabilization phase (Fig. 2). However, this relationship does not hold for all models, pointing to other dominant processes that may be at play, such as the evolution of physical feedbacks, heat uptake by the ocean, carbon uptake by the ocean and land sinks, and the fraction of radiative forcing explained by CO_2 compared to non-CO_2 agents (e.g. Williams et al., 2017, 2020).

When summed from 1850 to 2150, the total CO_2-fe emissions amount to 1063 (750 to 1461) PgC for the 1.5 ºC target and 1380 (1087 to 1785) PgC for the 2.0 ºC target. The lower end of the multi-model distribution encompasses the estimate of 817 PgC, respectively 1090 PgC found by Mengis and Matthews (2020) under a 1.5 ºC and 2.0 ºC stabilisation scenario with the UVic model.

Similar to residual emissions compatible with temperature stabilization, the spread across models in EB_{2026} and its evolution is very large. For the 1.5 °C target, this range spans from a decrease of a factor of -1.2 to an increase of a factor of 6.9 between 2025 and 2100-2150. The largest decrease in absolute value is simulated by CESM2, for which EB_{2026} is initially estimated at 100 PgC, but decreases drastically to 6 PgC by 2100-2150 for the 1.5 ºC target. The largest increase is simulated by GFDL-ESM4, for which EB_{2026} is initially 111 PgC but increases sharply to 475 PgC. For the 2 °C target, the factor spans from 0.8 to 2.4.

This large range in EB_{2026} reflects the uncertainties in the non-linear evolution of the TCRE, in the response to non-CO_2 forcing agents but also in internal climate variability. The range in EB_{2026}, when estimated at the end of year 2025, across the ensemble members of GFDL-ESM2M, represents 41 % (24 %) of the total model range for the 1.5 ºC (2.0 ºC) target (Fig. B4). For EC-Earth, the ensemble range amounts to 28 % (11 %) of the total model range. These differences are predominantly caused by differences in GSAT anomaly across members. If a perfect fit to GSAT for anthropogenic warming existed, which could remove all internal variability, these differences would vanish. This shows how sensitive the emission budget is to the estimate of global warming (Tokarska et al., 2020). When EB_{2026} is re-estimated later in the simulations and averaged between 2100 and 2150, the GFDL-ESM2M range is 41 % (44 %) of the model range and the EC-Earth ensemble amounts to 24 % (31 %).

As the evolution in the remaining emission budget is crucial for achieving the Paris Agreement goals, we here test if this evolution can be explained by standard climate metrics, such as the (effective) Equilibrium Climate Sensitivity (ECS), the Transient Climate Response (TCR) and the (CO_2-only) Transient Climate Response to cumulative CO_2 emissions (TCRE). These metrics, reported by various studies (Arora et al., 2020; Meehl et al., 2020; MacDougall et al., 2020) are analyzed alongside the 2025 estimate of the TCRE-fe including all CO_2-fe emissions. For the 2.0 ºC target, there is no significant

https://doi.org/10.5194/egusphere-2024-488
Preprint. Discussion started: 28 February 2024

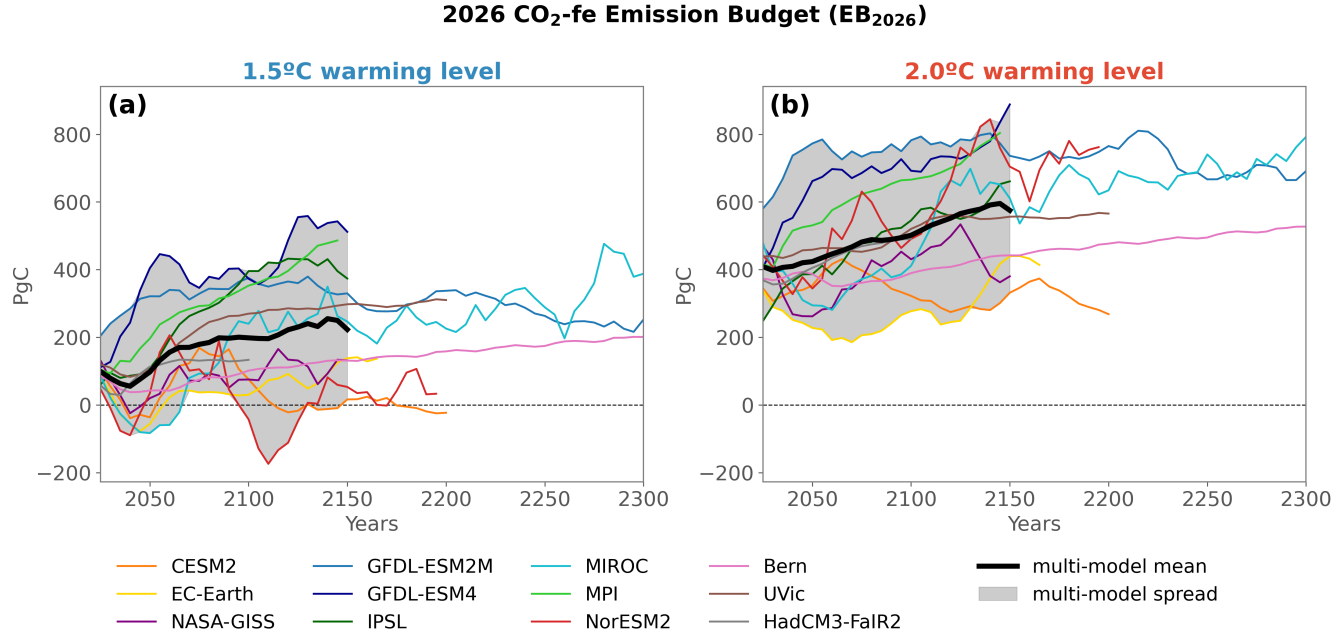

Figure 4. Remaining CO_2-fe Budget recalculated from the beginning of year 2026 at each stocktake (denoted as EB_{2026} in the text) in the 1.5 ºC (a) and 2.0 ºC (b) target simulations. The ensemble mean is shown for models that have several ensemble members. The multi-model mean is displayed by the black thick line and the grey shading covers the min-max spread.

relationship between those metrics and the differences in EB_{2026} between the 2100-2150 average and the first estimate at the end of 2025 (Fig. 5). The IPSL model stands out as being a highly sensitive model (Boucher et al., 2020), thus with a very low initial estimate of the EB_{2026} compared to other models. However, as emissions rapidly decrease during the AERA simulations, the linearity of the TCRE-fe relationship breaks in this model and positive emissions become necessary to keep warming the model at the target temperature. This could be due either to large negative ZEC (which needs to be confirmed by dedicated ZECMIP simulations), and/or to strong sensitivity to non-CO_2 greenhouse gases which are heavily mitigated in the SSP1-2.6 scenario. When the IPSL model is removed from the analysis, a clearer relationship emerges. Models with higher sensitivity (e.g., high ECS/TCR/TCRE/TCRE-fe) tend to exhibit a lower increase or even a slight decrease in the EB_{2026}, while less sensitive models show a more substantial increase. It is noticeable that the relationship between the different configurations of the Bern model (small pink dots) aligns particularly well with the slope of the linear regression between models excluding IPSL (red line). This relationship aligns with previous findings illustrating a positive correlation between the zero emissions commitment (implying decreases in EB over time) and TCR or TCRE across multiple models (MacDougall et al., 2020). Additionally, this correlation is evident between the zero emissions commitment and ECS within parameter-perturbed ensembles of a single model (MacDougall et al., 2020), as also shown here for the Bern model. Nevertheless, this relationship is not true for all models as shown in Fig. 5 and the range remains large. For example, NASA-GISS has a low

https://doi.org/10.5194/egusphere-2024-488
Preprint. Discussion started: 28 February 2024

sensitivity but a decreasing EB_{2026}. As pointed out by MacDougall et al. (2020), the evolution of the surface temperature and thus the evolving amount of emissions needed to stabilize warming is a balance between large quantities controlled by heat and carbon dynamics, and thus not expected to scale particularly well with these climate metrics.

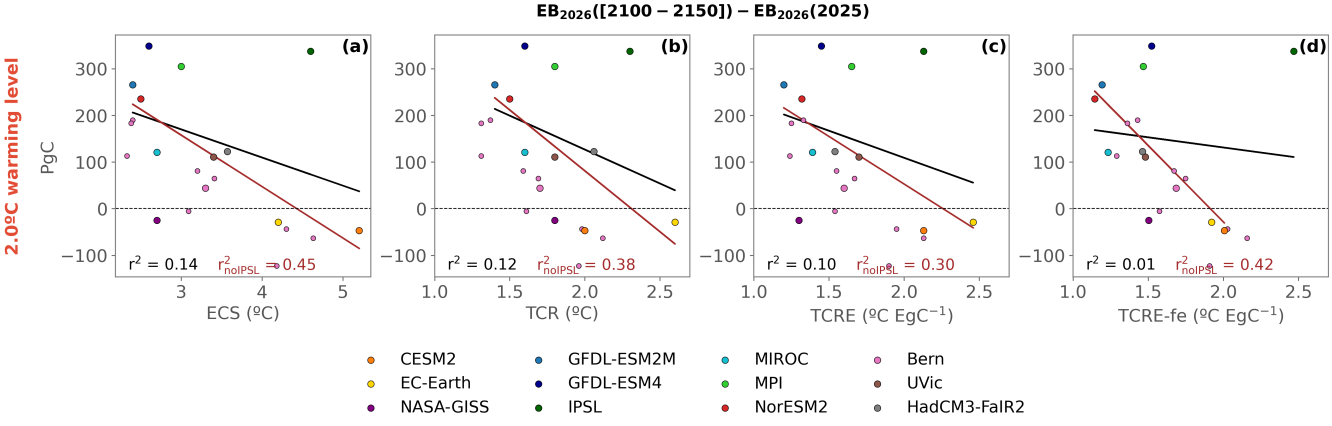

Figure 5. Simulated changes in the EB_{2026} between the estimate averaged over 2100-2150, and the first estimate at the end of year 2025, plotted against ECS (a), TCR (b), CO_2-only TCRE (c) and TCRE-fe at the end of year 2025 (d). Here only the 2.0 ºC simulation is shown. Results for the 1.5 ºC simulation are displayed in Fig. B5. The black line indicates the linear regression including all models, and the red line excluding the IPSL model. The 9 parameter-perturbed configurations of the Bern model are displayed by the small pink dots but the regression is calculated based on the ensemble mean (larger pink dot).

5 Where does the carbon go?

5.1 Global response

Atmosphere, ocean and land carbon fluxes exhibit peak and decline patterns, albeit with distinct differences between all three sinks (Fig. 6). In this section, our emphasis is on the 2.0 ºC scenario. However, the analysis for the 1.5 ºC scenario is shown in the Appendix (Fig. B6), and the numbers for the cumulative emissions and sinks are reported for both scenarios in Tables 3 and 4.

The atmospheric CO_2 growth rate, G_{ATM}, initially mirrors fossil fuel emissions, reaching 4.7 (3.5 to 5.7) PgC yr^{-1} in 2020 (Fig. 6a), consistent with the observation-based estimate of 5.0 $\pm$ 0.2 PgC yr^{-1} (Friedlingstein et al., 2022). As emissions decrease, G_{ATM} deviates from fossil fuel emission trends, turning negative and reaching -0.5 (range: -2.7 to 1.7) PgC yr^{-1} between 2100-2150 due to continued carbon uptake by the ocean and land. The ocean remains a consistent carbon sink, with multi-model mean uptake decreasing from 2.9 (2.2 to 3.3) PgC yr^{-1} in 2020 to 1.2 (0.2 to 1.9) PgC yr^{-1} by 2100-2150 (Figs. 6c). Conversely, the net land carbon sink (S_{LAND}-E_{LUC}) undergoes a transition from a net source to a sink between 1850-1950. The net land carbon sink peaks at 2.1 (0.5 to 4.1) PgC yr^{-1} in 2020 and remains a net sink or neutral until 2200 (Fig. 6g).

https://doi.org/10.5194/egusphere-2024-488
Preprint. Discussion started: 28 February 2024

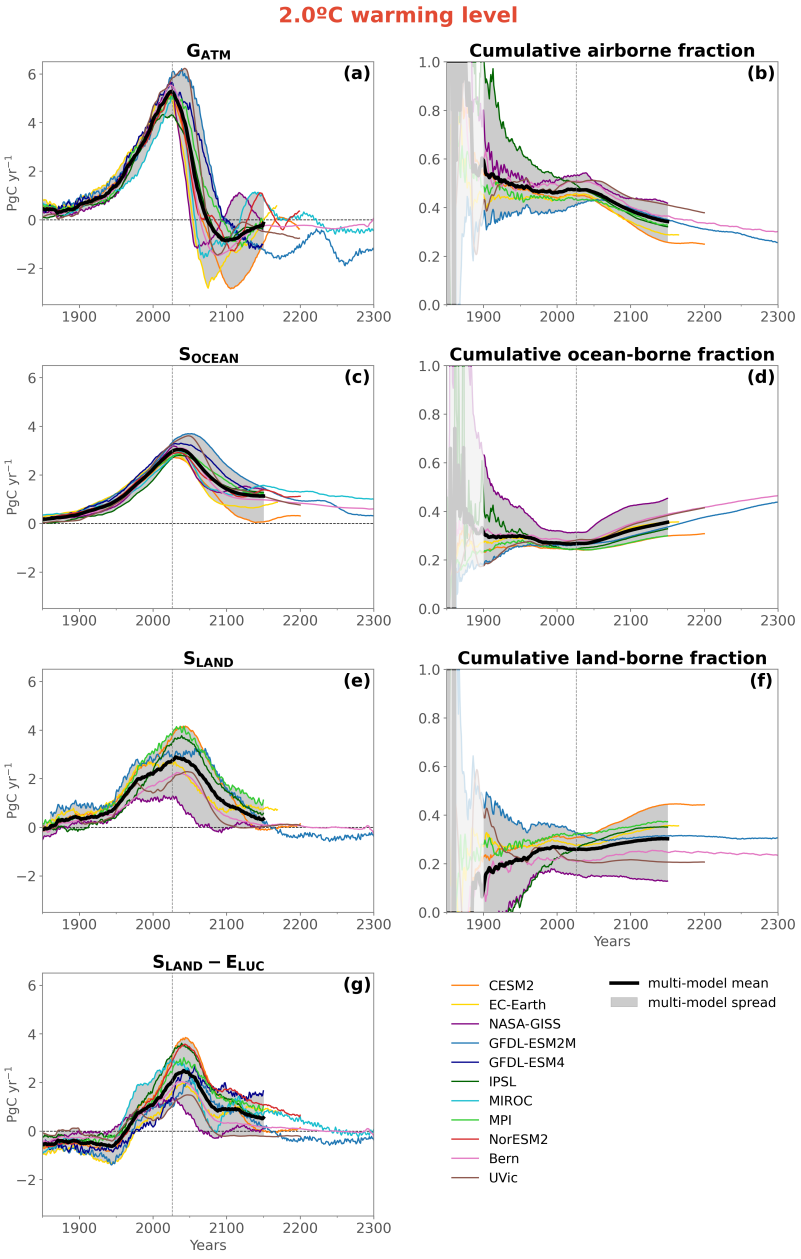

Figure 6. (a) Atmospheric CO_2 growth rate (G_{ATM}), (c) net ocean sink (CO_2 flux into the ocean; S_{OCEAN}), (e) gross land sink (S_{LAND}), (g) net land sink (CO_2 flux into land; S_{LAND} - E_{LUC}), cumulative (b) airborne, (d) ocean-borne and (f) land-borne fractions, in the 2.0 ºC simulation. The multi-model mean is displayed by the black thick line and the grey shading covers the min-max spread. Apart from the cumulative fractions, all time series have been smoothed with a 31-year running mean to remove short-term internal variations for visual purposes. The numbers are reported in the text without the 31-year average to be comparable with the Global Carbon Budget estimates.

https://doi.org/10.5194/egusphere-2024-488
Preprint. Discussion started: 28 February 2024

Notably, the land sink reaches a neutral state faster than the ocean sink, even temporarily shifting to a small carbon source by the end of the 22nd century. The simulated ocean and land carbon uptake in 2020 align well with the observation-based estimates: 3.0 ± 0.4 PgC for ocean carbon uptake and 2.0 PgC yr^{-1} (S_{LAND} = 2.9 ± 1.0 PgC yr^{-1} minus E_{LUC} = 0.9 ± 0.7 PgC yr^{-1}) for land carbon uptake (Friedlingstein et al., 2022). Among the models providing land use change emissions estimates, the gross land carbon uptake S_{LAND} emerges as a larger sink than the net land carbon flux $S_{LAND} - E_{LUC}$ (Fig. 6e), trending towards neutrality or even displaying a source tendency on longer timescales in GFDL-ESM2M. S_{LAND} in NASA-GISS, which lies at the lower end of the model range, is small because its sensitivity to CO_2 fertilization is damped: while the model simulates enhanced photosynthetic uptake of CO_2, its vegetation structure remains fixed and the extra carbon is instead allocated to the soil where it can still be respired back to the atmosphere. Also, it does not capture regrowth from secondary forest. These together lead to a relatively smaller cumulative land-borne fraction (Fig. 6d) and larger cumulative ocean-borne fraction by compensation (Fig. 6d).

The net ocean carbon flux initially has a narrow spread across models during the historical period, with a min-max range of 0.8 PgC yr^{-1} over 2000-2020. However, this spread notably widens after 2025, reaching 1.5 PgC yr^{-1} over 2040-2060 and 1.7 PgC yr^{-1} over 2100-2150. Pre-2025 differences among models are mainly due to various representations of ocean circulation and biogeochemistry in ESMs (Terhaar et al., 2022b). Post-2025, the widening spread results also from differing emission pathways. In contrast, the land carbon flux exhibits a much wider spread during the historical period, reaching 4.0 PgC yr^{-1} over 2000-2020. This range only increases slightly after 2025 to 5.0 PgC yr^{-1} over 2040-2060, reverting to 4.0 PgC yr^{-1} over 2100-2150. The substantial spread in land carbon flux, not entirely depicted in Fig. 6 due to a 31-year average for visual clarity, arises from the diverse representations of land carbon processes across models (Canadell et al., 2021).

From 1850 to 2020, 294 (236 to 354) PgC of the cumulative CO_2 emissions from fossil fuel (462 PgC, Table 3) and land use change (170 PgC) stayed in the atmosphere, while the ocean has taken up 173 (128 to 208) PgC, and the land absorbed 168 (79 to 254) PgC (Table 4). This partitioning translates to a cumulative airborne fraction of 0.48 (0.41 to 0.53), an ocean-borne fraction of 0.27 (0.24 to 0.31) and a land-borne fraction of 0.26 (0.16 to 0.33). These values are similar to observation-based estimates for 1850-2020 of 0.26 for the ocean sink and 0.30 for the land sink (Friedlingstein et al., 2022). Over the simulation period, the cumulative airborne fraction steadily decreases alongside declining emissions after 2025, signifying the gradual uptake of anthropogenic carbon by the ocean and the land (Fig. 6b,d,f). By the year 2150, the cumulative airborne fraction decreases to 0.34 (0.26 to 0.42), with an average of 416 (284 to 354) PgC of anthropogenic carbon still remaining in the atmosphere. Concurrently, the ocean-borne fraction consistently rises, emerging as the dominant fraction by the end of the simulations. In 2150, the ocean-borne fraction increases to 0.36 (0.30 to 0.45), surpassing both the land-borne fraction of 0.30 (0.13 to 0.44) and the airborne fraction. The cumulative ocean sink by 2150 amounts to 426 (330 to 556) PgC, while the land has taken up 370 (113 to 540) PgC. Nonetheless, substantial variability persists among model estimates for each fraction.

5.2 Regional distribution

The continuous ocean carbon uptake until the end of the simulations is limited to specific regions (Fig. 7a,c,d). While the ocean carbon sink increases almost everywhere from the early 20th century to the mid-21st century, it only continues to take up

https://doi.org/10.5194/egusphere-2024-488
Preprint. Discussion started: 28 February 2024

Table 3. Cumulative E_{FOS} and E_{LUC} emissions in 2020 and 2150.

Models	**E_{FOS} (PgC)**			**E_{LUC} (PgC)**	
	2020	**2150 1.5ºC**	**2150 2.0ºC**	**2020**	**2150**
CESM2	460	522	800	210	242
EC-Earth (3 members)	460	563 (509 ; 629)	760 (672 ; 841)	311	334
NASA-GISS	467	511	841	42	40
GFDL-ESM2M (5 members)	452	839 (747 ; 919)	1240 (1166 ; 1373)	309	425
GFDL-ESM4	467	925	1227	/	/
IPSL (2 members)	465 (465 ; 465)	841 (839 ; 843)	1049 (1033 ; 1065)	72	92
MIROC	461	641	966	/	/
MPI	467	845	1146	204	293
NorESM2	461	491	1088	/	/
Bern (72 members)	459	604 (356 ; 867)	899 (615 ; 1259)	110	128
UVic	472	765	1021	103	173
Mean (min-max)	**462 (452 ; 472)**	**685 (490 ; 925)**	**1002 (759 ; 1239)**	**170 (41 ; 310)**	**215 (215 ; 425)**

carbon after temperature stabilization at the end of the 21st century in the Southern Ocean and the low latitude regions close to the equator. Especially the Southern Ocean around 60ºS remains a prominent and enduring carbon sink post temperature stabilization, a consistent feature across models (no stippling in Fig. 7a,d). Cumulatively, the Southern Ocean south of 30ºS, representing 35 % of the ocean area, takes up 42 % (35 % to 46 %) of the global ocean carbon uptake by 2020, rising to 46 % (35 % to 57 %) by 2150 in the 2.0ºC simulation shown here. This region remains a sink until 2300 for the models that have run long simulations (GFDL-ESM2M, MIROC, Bern, not shown). Another strong present-day carbon sink (panel c), the subpolar North Atlantic, ceases to absorb carbon when the surface temperature stabilizes (panel d). The subpolar North Atlantic north of 40ºN (and using the northern boundary of Fay and McKinley (2014)) represents 3 % of the ocean area, but takes up 7 % (3 % to 11 %) of global ocean carbon uptake by 2020, a fraction that decreases to 5 % (1 % to 11 %) by 2150. The prevalence of the Southern Ocean carbon sink is consistent with results from CMIP5 and CMIP6 simulations for the historical period and for idealized 1pctCO_2 experiments (Frölicher et al., 2015; Terhaar et al., 2021; Williams et al., 2023). The pronounced long-term steady carbon sink in the Southern Ocean can be attributed to the high carbon concentration feedback and efficient surface to deep export of anthropogenic carbon shown in earlier studies (Tjiputra et al., 2010; Roy et al., 2011). In the mid-latitude

https://doi.org/10.5194/egusphere-2024-488
Preprint. Discussion started: 28 February 2024

Table 4. Cumulative G_{ATM}, S_{OCEAN} and S_{LAND} sinks in 2020 and 2150. S_{LAND} values can only be diagnosed for models which have provided an estimate of their simulated E_{LUC} (see Methods).

Models	**G_{ATM} (PgC)**			**S_{OCEAN} (PgC)**			**S_{LAND} (PgC)**		
	2020	**2150 1.5ºC**	**2150 2.0ºC**	**2020**	**2150 1.5ºC**	**2150 2.0ºC**	**2020**	**2150 1.5ºC**	**2150 2.0ºC**
CESM2	308	172	284	166	257	330	207	383	492
EC-Earth	354	231	318	209	328	391	220	345	392
(3 members)	(348 ; 360)	(205 ; 262)	(269 ; 363)	(207 ; 210)	(304 ; 347)	(362 ; 411)	(214 ; 227)	(332 ; 354)	(376 ; 400)
NASA-GISS	272	204	369	160	292	400	80	57	113
GFDL-ESM2M	309	375	582	197	451	557	254	435	521
(5 members)	(299 ; 313)	(340 ; 401)	(532 ; 661)	(196 ; 198)	(426 ; 478)	(540 ; 582)	(250 ; 261)	(400 ; 467)	(504 ; 553)
GFDL-ESM4	331	392	550	206	426	509			
IPSL	256	295	370	123	318	378	128	312	404
(2 members)	(256 ; 256)	(294 ; 296)	(362 ; 378)	(123 ; 123)	(314 ; 322)	(374 ; 382)	(128 ; 128)	(311 ; 313)	(399 ; 409)
MIROC	236	212	349	171	316	406			
MPI	299	330	475	166	348	433	214	468	540
NorESM2	292	140	416	183	271	424			
Bern	290	241	375	160	300	398	122	191	254
(72 members)	(282 ; 301)	(137 ; 347)	(245 ; 557)	(152 ; 166)	(227 ; 387)	(299 ; 507)	(118 ; 126)	(121 ; 263)	(175 ; 340)
UVic	293	349	488	161	371	455	124	213	245
Mean	**294**	**267**	**416**	**173**	**335**	**426**	**168**	**300**	**370**
(min-max)	**(236 ; 354)**	**(139 ; 354)**	**(284 ; 354)**	**(128 ; 208)**	**(256 ; 450)**	**(330 ; 556)**	**(79 ; 254)**	**(56 ; 468)**	**(113 ; 540)**

subtropics, some models even simulate less carbon uptake or outgassing due to the accumulation of anthropogenic carbon near the surface layers (Couespel and Tjiputra, 2024; Rodgers et al., 2020).

The land carbon uptake also persists only in particular regions during temperature stabilization (Fig. 7b,e,f). Some strong and robust carbon sink regions in the present era (2011-2030), particularly in tropical areas like South America, central Africa and part of Indonesia, experience a complete cessation of carbon uptake after 2100. However, strong terrestrial carbon uptake persists in the Northern Hemisphere during temperature stabilization, including regions like Central America, temperate and boreal forests in Eastern North America and Eurasia.

Compared to the ocean carbon uptake, the land carbon uptake has locally a larger uncertainty across models, although much of this uncertainty is located in regions where no carbon exchange is found during the pre-industrial period (e.g. desertic regions), and is thus not indicated by stipples on the maps (see caption in Fig. 7).

The land and ocean carbon sink patterns look qualitatively similar as previous results based on low emission scenarios (Canadell et al., 2021). The novelty of these simulations is a quantification of these sinks for a given temperature target and the representation of carbon cycle dynamics beyond the 21st century under strong mitigation scenarios. For example, here we

https://doi.org/10.5194/egusphere-2024-488
Preprint. Discussion started: 28 February 2024

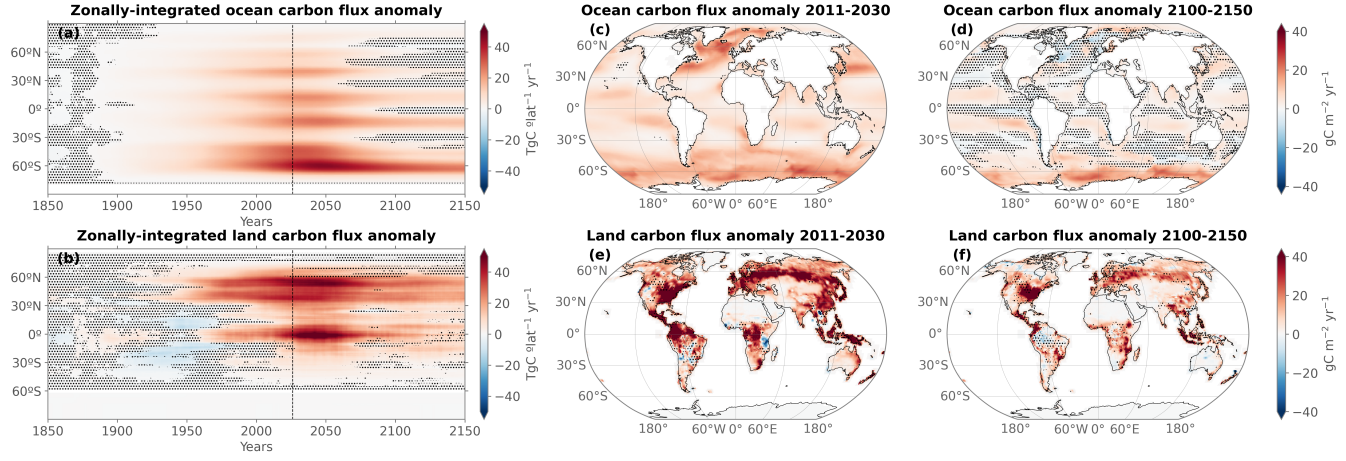

Figure 7. Multi-model mean ocean (top, S_{OCEAN}) and land (bottom, $S_{LAND} - E_{LUC}$) carbon flux anomalies in the 2.0ºC simulation relative to 1850-1900. In panels (a) and (b) the fluxes are zonally-integrated and smoothed with a 31-year running mean, while panels (c)-(f) display maps averaged between 2011-2030 and 2100-2150. Stipples indicate where less than 80 % of the models agree on the sign of the anomaly. Stippling is not shown where carbon fluxes during the 1850-1900 period are lower than 2.5 gC m^{-2} yr^{-1}.

show that the North Atlantic ocean sink vanishes during and after stabilization while the Southern Ocean remains an active sink. The divergence in carbon uptake between these regions can be attributed to distinct ocean circulation patterns. The Southern Ocean is the region where old, anthropogenic CO_2-poor circumpolar deep waters are being upwelled (e.g. Mikaloff Fletcher et al., 2006), even during global surface climate stabilization. This upwelling results in continuous carbon uptake due to the positive air-sea gradient in anomalous pCO_2 (Frölicher et al., 2015). On the other hand, when global temperature stabilizes, the Atlantic Meridional Overturning Circulation (AMOC) is expected, at least in some models, to recover after an initial decrease (e.g. Manabe and Stouffer, 1994; Sigmond et al., 2020; Frölicher et al., 2020; Schwinger et al., 2022; Bonan et al., 2022), a phenomenon associated with a recovery of deep convection in the subpolar North Atlantic, enhanced mixing of anthropogenic CO_2-rich waters previously sequestered at depth, and a consequently lower ocean carbon uptake in this region. A stronger AMOC would also transport more warm surface waters with high anthropogenic carbon concentrations to the high latitudes where the anthropogenic carbon would be outgassed during cooling (Siegenthaler and Joos, 1992; Völker et al., 2002; Tjiputra et al., 2010), a phenomenon already simulated for the present time in the Arctic Ocean while atmospheric CO_2 is still increasing (Terhaar et al., 2020). The exact drivers of the vanishing Atlantic Ocean carbon sink under temperature stabilization will be the subject of future dedicated studies using the AERA-MIP simulations.

https://doi.org/10.5194/egusphere-2024-488
Preprint. Discussion started: 28 February 2024

6 Discussion

The AERA-driven simulations achieve temperature stabilization with realistic CO_2 emission pathways across an ensemble of comprehensive Earth System Models. However, applying the AERA with ESMs is more complex than traditional concentration-driven simulations and comes with its caveats and limitations.

We robustly quantify a decrease in CO_2-fe emissions towards very low emissions for the selected 1.5 ℃ and 2.0 ℃ warming targets. To which extent reductions in CO_2-fe emissions are realized by reductions in emissions of fossil fuel CO_2 vs other agents depends on scenario choices. We opted for the low emission high mitigation scenario SSP1-2.6 for all greenhouse gases except CO_2. While the choice does not impact initial estimates of the REB and CO_2-fe emission pathways (Terhaar et al., 2022a), it does affect fossil fuel CO_2 emissions, atmospheric CO_2 and the land and ocean carbon sinks (Terhaar et al., 2023). Thus, the quantitative estimates presented here for the carbon distribution and atmospheric CO_2 offer a likely pathway under low emissions and high mitigation but may not encompass all uncertainties. These estimates may change if alternative trajectories for non-CO_2 radiative agents and land use change are pursued in the future. Nevertheless, qualitative statements remain robust, such as the necessity to substantially reduce fossil fuel CO_2 emissions for temperature stabilization and the continuous carbon uptake by the Southern Ocean even under temperature stabilization.

The choice of the scenario for non-CO_2 radiative agents can also lead to unwanted trajectories of the CO_2 emission curve if the prescribed non-CO_2 scenario is not ideal for the chosen temperature target. In the case of the 2°C target, CO_2 emissions increase from 2025 to 2030 and start to decrease strongly afterwards (Fig. 2f). The temporal increase in fossil fuel CO_2 emissions is a result of a strong decline in CO_2-fe emissions from declining non-CO_2 radiative agents under SSP1-2.6, which exceeds the necessary total CO_2-fe emission decline calculated by the AERA in 2025. As a result, fossil fuel CO_2 emissions increase to compensate for the strong decline in CO_2-fe emissions from declining non-CO_2 radiative agents. Such unwanted effects could be avoided by adjusting the SSP1-2.6 scenario so that mitigation efforts of non-CO_2 agents and land use start later, as already applied by Millar et al. (2017), or simply by choosing the best fitting non-CO_2 SSP scenario for each temperature target. Another possibility which might be offered in the future when ESMs develop an emission-driven mode for non-CO_2 agents is to scale the CO_2 and non-CO_2 emissions, as already applied in Terhaar et al. (2022a) with an EMIC.

The non-CO_2 and land use change emissions do not only add uncertainties to the carbon budget but also add uncertainties to the AERA at each stocktake. At each stocktake, the AERA needs information about the CO_2-fe emissions from non-CO_2 radiative agents and from land use change. Unfortunately, most models do not provide emissions from land use change or the non-CO_2 radiative forcing from which the corresponding CO_2-fe emissions can be estimated. As a result, the CO_2-fe emissions from land use change and from non-CO_2 agents provided to AERA are estimated from another source (see Methods), which lead to discrepancies between the real CO_2-fe emissions in the model and the estimated CO_2-fe emissions seen by the AERA. This discrepancy affects the estimate of the TCRE-fe and the future CO_2 emission curve, which is estimated as the difference between the AERA-derived CO_2-fe emission curve and the CO_2-fe emissions from land use change and non-CO_2 radiative agents. Fortunately, the simulations provided here with an ensemble of ESMs demonstrate that the re-evaluation of the TCRE-fe and the future CO_2-fe emission curve every 5 years allows all models but one to reach the temperature target without any

https://doi.org/10.5194/egusphere-2024-488
Preprint. Discussion started: 28 February 2024

larger divergence (Fig. 2). For future simulations, possibly within CMIP7, diagnosing each models' effective radiative forcing of non-CO_2 agents and land use change (Smith, 2020; Zelinka et al., 2023) would likely lead to even more precise results, as shown in more detail for the IPSL model in Appendix A. This is particularly important for the aerosol radiative forcing, which is the most uncertain component, with important repercussions for the ability to reach climate goals (Watson-Parris and Smith, 2022).

Not only the implementation of the AERA with ESMs introduces uncertainties, but the ESMs themselves also have limitations. Potential feedbacks such as thawing permafrost (MacDougall and Friedlingstein, 2015; MacDougall et al., 2015; Burke et al., 2017; Gasser et al., 2018; Lowe and Bernie, 2018; MacDougall, 2021), peat land area and carbon evolution (Müller and Joos, 2021), ocean circulation changes due to ice melt from Greenland or Antarctica (Bronselaer et al., 2018; Lago and England, 2019; Li et al., 2023), feedbacks between warming, nitrous oxide and methane (Stocker et al., 2013; Battaglia and Joos, 2018; IPCC, 2021), and, on longer timescales than considered in this study, feedbacks associated with the potential melting and disintegration of polar ice sheets are currently missing from most ESMs. These feedbacks would potentially reduce the emission budget over time and potentially make negative emissions over long time periods necessary to maintain a stable temperature (Palazzo Corner et al., 2023).

7 Conclusions

This study presents multi-ESM emission-driven projections compatible with internationally-agreed climate goals. We showed that the Adaptive Emission Reduction Approach (AERA) proposed by Terhaar et al. (2022a) works not only for EMICs but also for more complex, higher-resolution fully-coupled ESMs. The temperature targets are reached even when the simulated non-CO_2 radiative forcing and land use change emissions are not fully known, with the exception of one ESM.

Unlike the standard CMIP scenarios that simulate different warming levels for the same prescribed CO_2 concentration or emission pathways (Tebaldi et al., 2021), all models converge to a given warming level. The convergence to a common warming level with varying emissions now allows to quantify the diversity of model responses in terms of emission pathways compatible with these warming levels, as well as resulting atmospheric CO_2 levels, carbon cycle responses, and their effect on ecosystems, such as ocean acidification (Terhaar et al., 2023). While globally integrated results are qualitatively similar to previous results with EMICs (Terhaar et al., 2022a, 2023; Goodwin et al., 2018b), the ESM simulations here allow to explore a more quantitative and regional focus, to better quantify uncertainties, and especially to quantify the importance of internal climate variability.

To limit warming to 1.5 ºC or 2.0 ºC (i.e., an allowable warming of 0.28 ºC and 0.78 ºC from year 2020 forward), drastic reductions in greenhouse gas emissions are necessary. If such immediate and drastic emission reductions of around -1 to -2 PgC yr^{-2} were implemented, both CO_2-fe and fossil fuel CO_2 emissions may even be allowed to stay positive (on the order of 1 PgC yr^{-1} upon stabilization). However, the amount of allowed continuous CO_2-fe emissions after the temperature is stabilized is strongly model-dependent, with a large spread found across ESMs. The large spread is mainly caused by varying zero emissions commitments and responses to non-CO_2 forcing agents across the model ensemble. Importantly, the negative

https://doi.org/10.5194/egusphere-2024-488
Preprint. Discussion started: 28 February 2024

multi-model mean zero emissions commitment might have a bias towards low values because of important feedback processes missing in most ESMs (e.g., the release of carbon from thawing permafrost).

The spread in the zero emissions commitment in combination with a non-constant TCRE-fe also results in an initially biased estimate of the remaining emission budget. On average across models, the REB that was estimated in 2025 could change by a factor of 1.4 to 2 (Table 2). The direction of change mainly depends on the ZEC, with a negative ZEC allowing for more emissions. Here, the REB was on average underestimated in line with a slightly negative multi-model mean ZEC (MacDougall et al., 2020). However, there are large uncertainties around the ZEC and hence the development of carbon and emission budgets with time.

A few ensemble simulations pointed to a significant role of internal variability, potentially explaining 30 % to over 50 % of the inter-model spread in compatible emissions, atmospheric CO_2 levels and emission budgets. The origin of this uncertainty partly lies in the estimate of the anthropogenic warming, which in practise differs among members and can lead to large differences in the emission budgets, as also pointed out by Tokarska et al. (2020). This indicates necessary caution when interpreting remaining budgets estimates, and planning for a margin of error in mitigation pathways to avoid overshooting the warming target.

In addition to the "relative target" simulations presented here (i.e., same amount of remaining warming for all models after 2020 based on observations), the AERA can also be used to make simulations with an "absolute target" (i.e. all models are set up to warm by the same amount relative to 1850-1900) or with an overshoot. Absolute target simulations allow to explore climate impacts of global surface temperature stabilization at different warming levels across Earth System Models (King et al., 2021), which will be the focus of future dedicated studies. Temperature overshoot simulations with the AERA allow to define the magnitude and length of the overshoot by varying temperature targets over time, e.g., a first temperature target of 2.0 ºC until 2050 followed by a step-wise reduction of that target every 5 years to 1.5 ºC in 2100 (Terhaar et al., 2022a).

The AERA framework proposed here only accounts for targets in global surface temperature, aligned with international climate agreements. However, other climate change impacts, such as ocean acidification, sea level rise, interior ocean changes, terrestrial productivity, regional extremes, pose important risks for ecosystem and human societies. Extending the AERA to other targets, and towards avoiding crossing some of the Earth's planetary boundaries (Rockström et al., 2009), as proposed by Steinacher et al. (2013); Seneviratne et al. (2016); Avrutin et al. (2023), would enable to constrain the emission budget and pathways towards a safer world.

The success of the AERA-MIP simulations across a large group of modeling centres shows that the AERA can be used in subsequent model intercomparison projects, such as CMIP7, with many applications for these temperature stabilization simulations.

Code and data availability. The AERA code is distributed as a python module openly available under https://github.com/Jete90/AERA, with a guided documentation and examples. The AERA-MIP model outputs used in this study are available under Silvy et al. (2024). The Python code used to produce the figures of this paper will be made openly available upon final publication.

https://doi.org/10.5194/egusphere-2024-488
Preprint. Discussion started: 28 February 2024

Appendix A: Further details on the AERA configuration of the participating models

All participating models are listed in Table A1. Both HadCM3-FaIR2 and MPI performed the AERA simulations with a previous version of the AERA code using an impulse response function to the radiative forcing to estimate anthropogenic temperature instead of the 31-year running mean (as in Terhaar et al. (2022a)). The HadCM3-FaIR2 configuration is described in details in Lee et al. (in review). Briefly, it uses the Hadley Centre Coupled Model version 3 (HadCM3, Collins et al. (2001)), with 29 members from a physics perturbed parameter ensemble (Sparrow et al., 2018). Because HadCM3 runs in concentration-driven mode and does not solve the carbon cycle, it is coupled to the Finite amplitude Impulse Response (FaIR) version 2 (Leach et al., 2021) at each AERA stocktake. The FaIR parameters are chosen to fit each member of the HadCM3 ensemble based on the 1881-2025 simulation period. The carbon cycle component of FaIR is used both to derive the CO_2-fe emissions from non-CO_2 agents, and to convert the CO_2 emissions given by AERA to CO_2 concentration to prescribe to HadCM3 every 5 years.

Model full name	Abbreviation	References	Simulated years	Ensemble members
ACCESS-ESM1-5	ACCESS	Ziehn et al. (2020)	1850-2200	1
CESM2	CESM2	Danabasoglu et al. (2020)	1850-2200	1
EC-Earth3-CC	EC-Earth	Döscher et al. (2022)	1850-2169	3
GFDL-ESM2M	GFDL-ESM2M	Dunne et al. (2012, 2013)	1861-2300	5
GFDL-ESM4	GFDL-ESM4	Dunne et al. (2020)	1850-2150	1
IPSL-CM6-LR-ESMCO2	IPSL	Boucher et al. (2020)	1850-2150	2
MIROC-ES2L	MIROC	Hajima et al. (2020)	1850-2300	1
MPI-ESM1-2-LR	MPI	Mauritsen et al. (2019)	1850-2150	1
NASA-GISS-E2-1-G-CC	NASA-GISS	Kelley et al. (2020); Ito et al. (2020); Miller et al. (2021); Lerner et al. (2024)	1850-2150	1
NorESM2-LM	NorESM2	Seland et al. (2020); Tjiputra et al. (2020)	1850-2200	1
Bern3D-LPX	Bern	Ritz et al. (2011)	1850-2300	72
UVic-ESCM-2.10	UVic	Mengis et al. (2020)	1850-2200	1
HadCM3-FaIR2	HadCM3-FaIR2	Lee et al. (submitted)	1881-2100	29

Table A1. Earth System Models of full and intermediate complexities participating in AERA-MIP.

The time series prescribed to AERA (default or model-estimated E_{LUC} and $E_{non\text{-}CO_2\text{-}fe}$) are listed in Table A2. To estimate their own simulated E_{LUC}, most models compare land-air carbon fluxes between two concentration-driven simulations following historical+SSP1-2.6 CO_2 concentrations (1850-2100), one with land use change activated and another without (Lawrence et al., 2016; Liddicoat et al., 2021). This difference is then smoothed with a 21-year running mean to remove large interannual variations. Eight models prescribed their internally-estimated E_{LUC} to AERA. The NASA-GISS model underestimates E_{LUC} as it estimated the emissions from land use change due to crop cover change only, but did not include the transport of crop

https://doi.org/10.5194/egusphere-2024-488
Preprint. Discussion started: 28 February 2024

615 harvest from land, and did not include the deforestation component of E_{LUC}. UViC used an estimate based on the carbon flux from vegetation burning only. The time series of all E_{LUC} estimates prescribed to AERA are shown in Fig. A2a.

Model	E_{LUC} **provided to AERA**	$E_{non\text{-}CO_2\text{-}fe}$ **provided to AERA**
ACCESS-ESM	Model estimate	Default
CESM2	Default	Default
EC-Earth	Model estimate	Default
GFDL-ESM2M	Default	Model estimate
GFDL-ESM4	Default	Model estimate from GFDL-ESM2M
IPSL-ESM	Default (r1i1p1f1) Model estimate (r1i1p2f1)	Default (r1i1p1f1) Model estimate (r1i1p2f1)
MIROC-ES2L	Default	Default
MPI-ESM	Model estimate	Default
NASA-GISS	Model estimate	Model estimate
NorESM2	Default	Default
Bern3D-LPX	Model estimate	Prescribed from SSP1-2.6
UVic-ESCM	Model estimate	Prescribed from SSP1-2.6
HadCM3-FaIR2	Model estimate	Model estimate

Table A2. AERA forcings prescribed to each model.

In the analysis of carbon distribution (Equation 5) presented in the paper, we corrected and re-estimated some of these E_{LUC} time series, to obtain the best estimate possible of the internally-simulated E_{LUC}. These time series are shown in Fig. A2b. GFDL-ESM2M performed a posteriori the concentration-driven simulations with and without land use change activated, 620 providing its estimate of E_{LUC} for the carbon analysis from 1861 to 2100. We then extended the time series to 2300 by applying a linear decay to zero emissions from 2100 to 2150, and maintaining the emissions at zero afterwards. We similarly corrected the MPI estimate between 2100 and 2150 by linearly decaying the emissions to zero. Dedicated UVic simulations were additionally performed to better estimate E_{LUC} in the AERA simulations for both targets. IPSL was also able to diagnose online the simulated E_{LUC} emissions within the AERA simulations. For CESM2, we were able to estimate E_{LUC} for the 625 historical period, using the available concentration-driven *hist* and *hist-nolu* simulations available on the Earth System Grid Federation and the method described above (Lawrence et al., 2016). However, the extension for the SSP1-2.6 scenario was not available. Nonetheless, the E_{LUC} term during the historical period matched the default E_{LUC} forcing from the Bern model adjusted time series (not shown), so we used the default estimate for the carbon distribution analysis.

The simulated effective radiative forcing from non-CO_2 agents was diagnosed in dedicated simulations for IPSL, but only 630 for CH_4, N_2O and aerosols, which have major climate impacts amongst non-CO_2 forcing agents. For other agents, we used the estimates from Smith et al. (2023) for the historical period and from Smith (2020) for the SSP1-2.6 scenario period post-2022.

https://doi.org/10.5194/egusphere-2024-488
Preprint. Discussion started: 28 February 2024

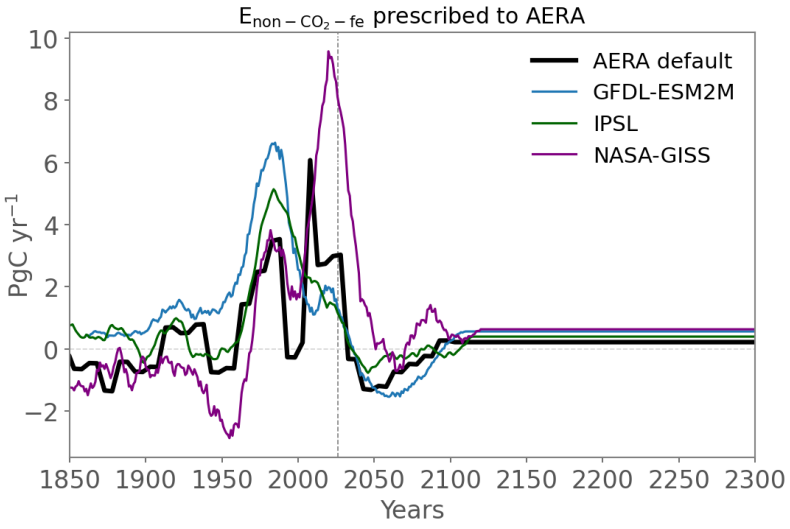

Figure A1. $E_{non\text{-}CO_2\text{-}fe}$ diagnosed in 3 models and default AERA input for the other models.

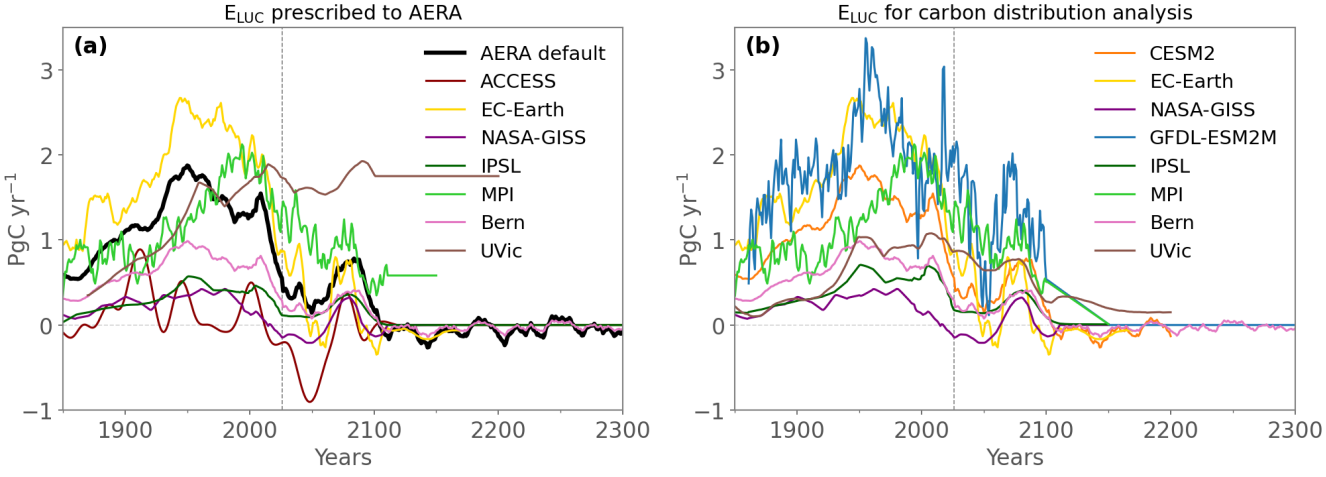

Figure A2. E_{LUC} diagnosed in the models and default AERA input. Panel a) shows the time series prescribed to AERA and panel b) the corrected time series used in the carbon distribution analysis of this paper (see text for details of the corrections).

For the IPSL model, one set of simulations were performed by prescribing the default $E_{non\text{-}CO_2\text{-}fe}$ and E_{LUC} forcings to AERA, while another set of simulations were performed with the internally-calculated emissions (Table A2), enabling us to test the effect of the mismatch in $E_{non\text{-}CO_2\text{-}fe}$ and E_{LUC} between the default time series and the internally-simulated emissions. The member with the internally-calculated emissions allowed for a shorter temperature undershoot in the 1.5 ºC simulation, and a better temperature stabilisation within the 2.0 ºC uncertainty range in the associated simulation. However, minor differences

https://doi.org/10.5194/egusphere-2024-488
Preprint. Discussion started: 28 February 2024

in emission budget and cumulative fossil fuel emissions were found overall between these two ensemble members, due to compensating effects between CH_4 and N_2O in the estimated and the internally-calculated radiative forcing, and between $E_{non\text{-}CO_2\text{-}fe}$ and E_{LUC}. As an indication, the $EB_{2026}(2025)$ (i.e., the REB from beginning of year 2026 estimated at the first stocktake) differs by 3 PgC for the 1.5 ºC target and by 15 PgC for the 2.0 ºC target between the two ensemble members. The differences increase to 52 PgC, respectively 48 PgC, for $EB_{2026}(2100-2150)$.

The simulations performed with the Bern3D-LPX model correspond to the configuration in Terhaar et al. (2023), where two parameters (ocean heat uptake efficacy and feedback parameter) were varied to obtain 9 values of Earth Climate Sensitivity (ECS) spanning the range 2.23 ºC to 4.63 ºC. Since Bern3D-LPX does not represent atmospheric variability on GSAT, a synthetic noise was added on the GSAT output read by AERA for each of these 9 ECS values, providing 8 synthetic ensemble members per configuration, hence a total of 72 ensemble members. This Bern3D-LPX range across members is thus more representative of parametric uncertainty, and not comparable to the perturbed initial-condition ensembles of EC-Earth and GFDL-ESM2M.

Appendix B: Additional figures

Author contributions. TLF, JT and FJ designed the AERA-MIP protocol. YS, FAB and FL participated in the testing and validation of the protocol. YS gathered and analyzed the simulations. YS, JT and TLF wrote the first draft of the manuscript. JT executed the Bern3D-LPX simulations. FAB and FL executed the GFDL-ESM2M simulations. JRB executed the CESM2 simulations. RF, VL and ET executed the EC-Earth3-CC simulations. PC executed the IPSL-CM6-LR-ESMCO2 simulations. MD and TL executed the ACCESS-ESM1-5 simulations. GG executed the MPI-ESM1-2-LR simulations. TH and MK executed the MIROC-ES2L simulations. NYK, PL and AR executed the NASA-GISS-E2-1-G-CC simulations. DL executed the HadCM3-FaIR2 simulations. NM and EAM executed the UVic-ESCM-2.10 simulations. JS and JT executed the NorESM2-LM simulations. ES executed the GFDL-ESM4 simulations. DP provided the GFDL-ESM2M radiative forcing from non-CO_2 radiative agents. All authors contributed to discussions and final writing of the manuscript.

Competing interests. All authors declare no competing interests.

Acknowledgements. This work was supported by the European Union's Horizon 2020 research and innovation program under grant agreement no. 821003 (project 4C). The work reflects only the authors' view; the European Commission and their executive agency are not responsible for any use that may be made of the information for the work. TLF (project Overshoot) and FJ (project Peakcarbon) also thank the CSCS Swiss National Supercomputing Centre for computing resources. TLF (PP00P2_198897), JT (PZ00P2_209044c), and FJ (200020_200511) have received funding from the Swiss National Science Foundation. JT has also received funding from the Woods Hole Oceanographic Institution Postdoctoral Scholar Program. EAM and NM are funded under the Emmy Noether scheme by the German Re-

https://doi.org/10.5194/egusphere-2024-488
Preprint. Discussion started: 28 February 2024

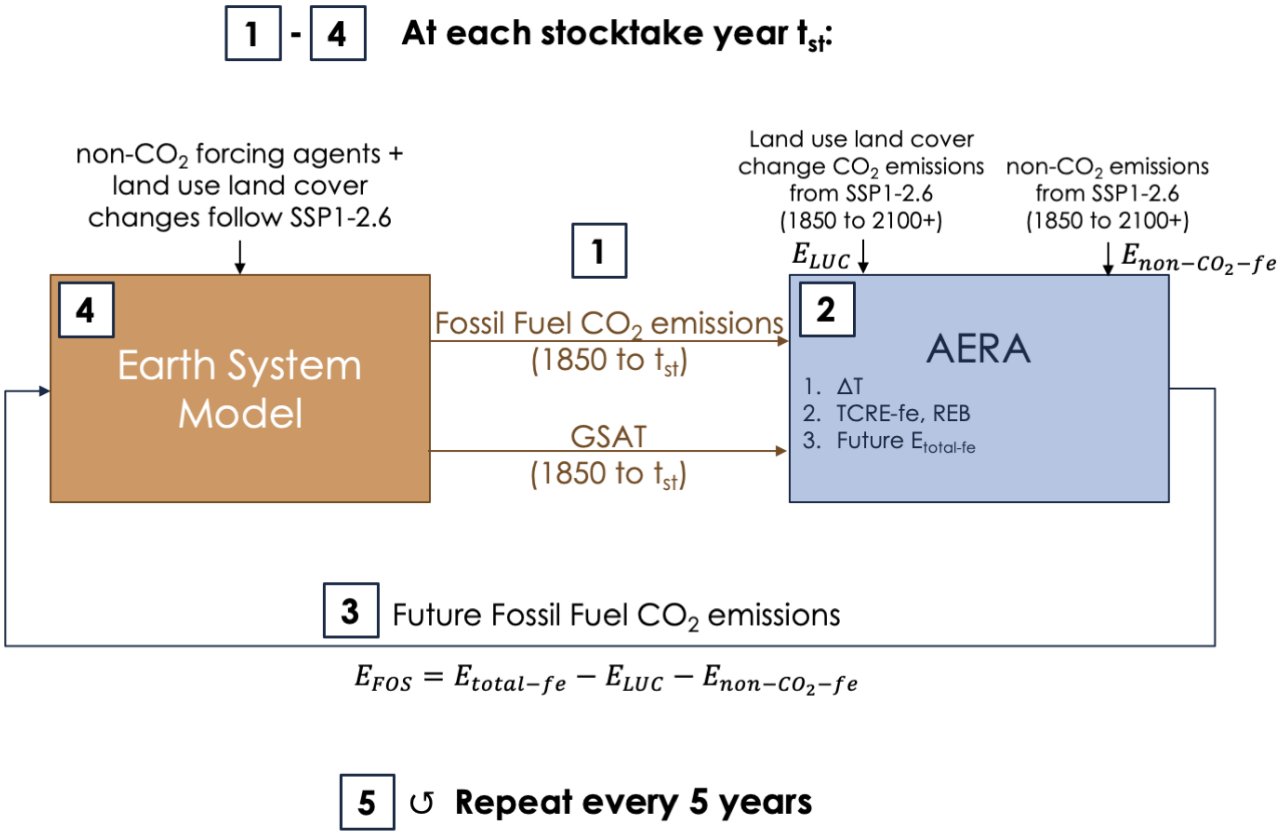

Figure B1. Schematic of the feedback loop between the Earth System Model and the AERA module. Steps 1 to 4 are performed at each stocktake year, starting at the end of 2025.

search Foundation 'FOOTPRINTS – From carbOn remOval To achieving the PaRIs agreemeNt's goal: Temperature Stabilisation' (ME 5746/1-1). GPP received funding from the European Union's Horizon Europe Research and Innovation Programme under grant agreement No 101081179 (DIAMOND). TZ receives funding from the Australian Government under the National Environmental Science Program (NESP). TH and MK were supported by the MEXT-Program for advanced studies of climate change projection (SENTAN, Grant Number JPMXD0722681344). TH was also supported by the Environment Research and Technology Development Fund (JPMEERF21S20820) of the Environmental Restoration and Conservation Agency provided by the Ministry of Environment of Japan. AR, PL, and NYK were supported by the NASA Modeling, Analysis and Prediction program, with computing resources provided by the NASA High-End Computing (HEC) Program through the NASA Center for Climate Simulation (NCCS) at Goddard Space Flight Center.

https://doi.org/10.5194/egusphere-2024-488
Preprint. Discussion started: 28 February 2024

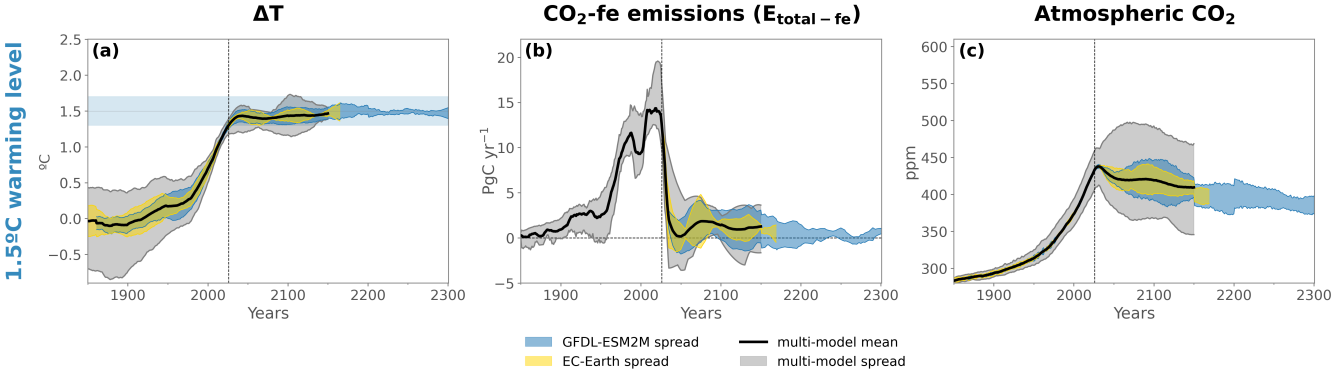

Figure B2. Same as Fig. 3 but for the 1.5 ºC target.

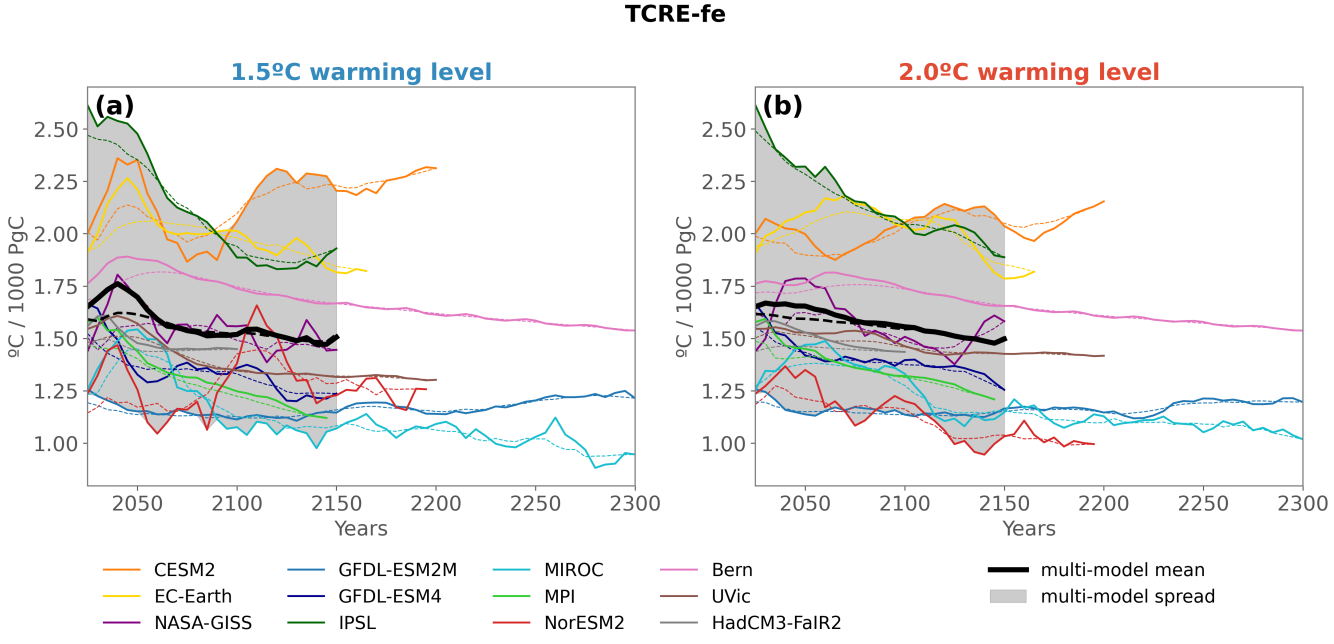

Figure B3. TCRE-fe calculated by AERA at each stocktake year (solid lines). Dotted lines indicate the TCRE-fe calculated a posteriori with the final ("true") estimate of the 31-year running mean timeseries of GSAT. This reconstructed TCRE-fe (dotted lines) is thus less variable than the TCRE-fe calculated by AERA which calculates ΔT based on the last year of the extended 31-year running mean timeseries until each stocktake year, which introduces some noise compared to the true final estimate.

https://doi.org/10.5194/egusphere-2024-488
Preprint. Discussion started: 28 February 2024

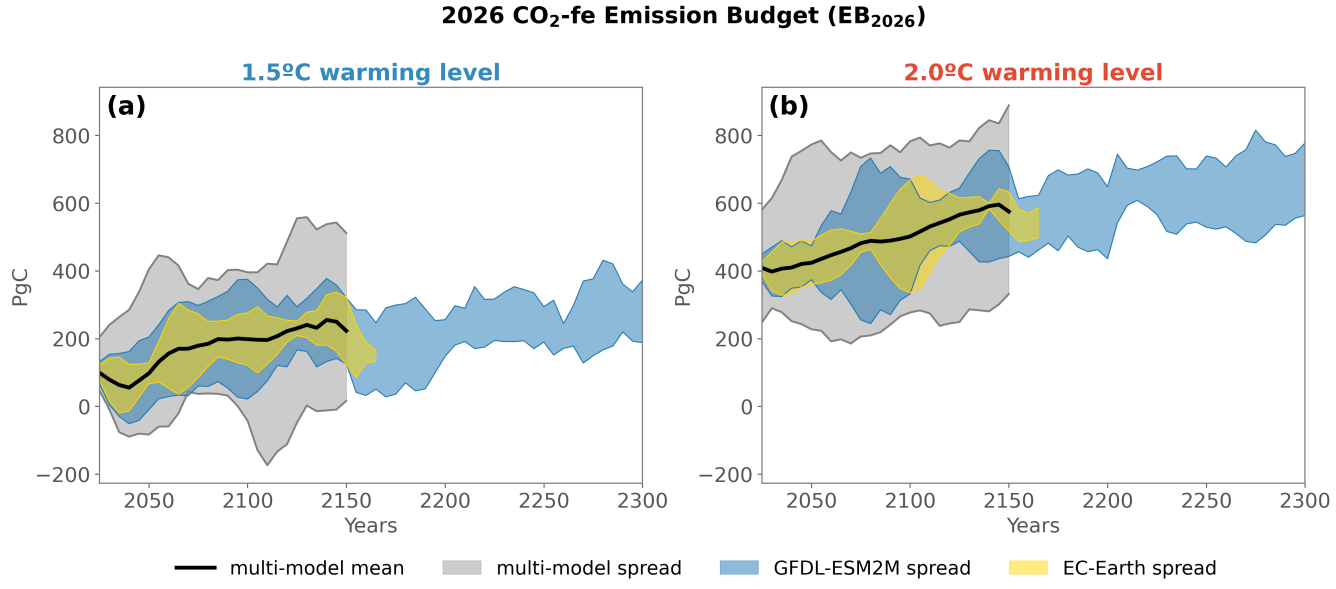

Figure B4. Same as Fig. 4 but showing only the multi-model mean and spread, as well as the min-max range across members for the GFDL-ESM2M and EC-Earth ensembles, centered on the multi-model mean.

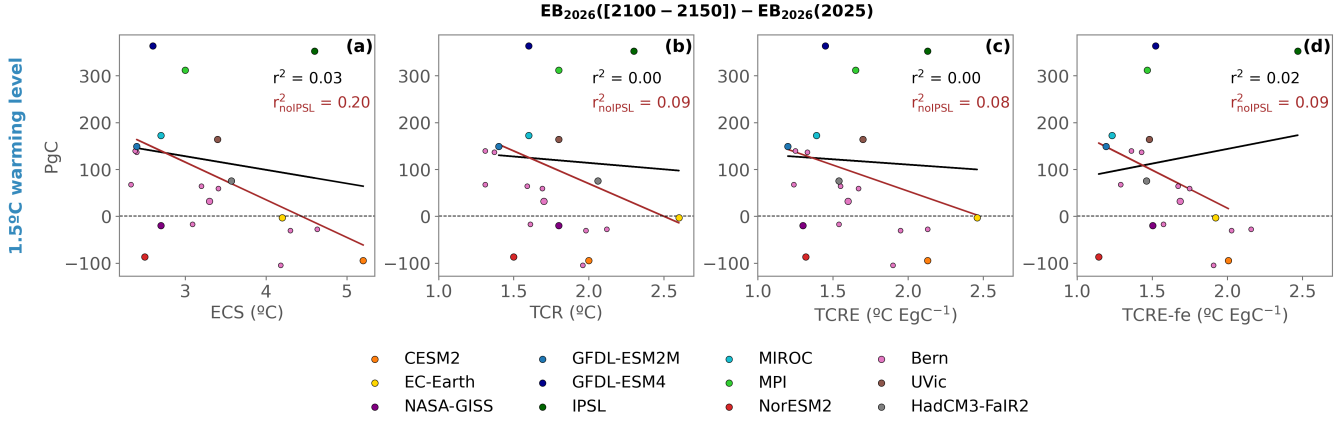

Figure B5. Same as Fig. 5 but for the 1.5 ºC target.

References

Allen, M. R., Frame, D. J., Huntingford, C., Jones, C. D., Lowe, J. A., Meinshausen, M., and Meinshausen, N.: Warming caused by cumulative carbon emissions towards the trillionth tonne, Nature, 458, 1163–1166, https://doi.org/10.1038/nature08019, number: 7242 Publisher: Nature Publishing Group, 2009.

https://doi.org/10.5194/egusphere-2024-488
Preprint. Discussion started: 28 February 2024

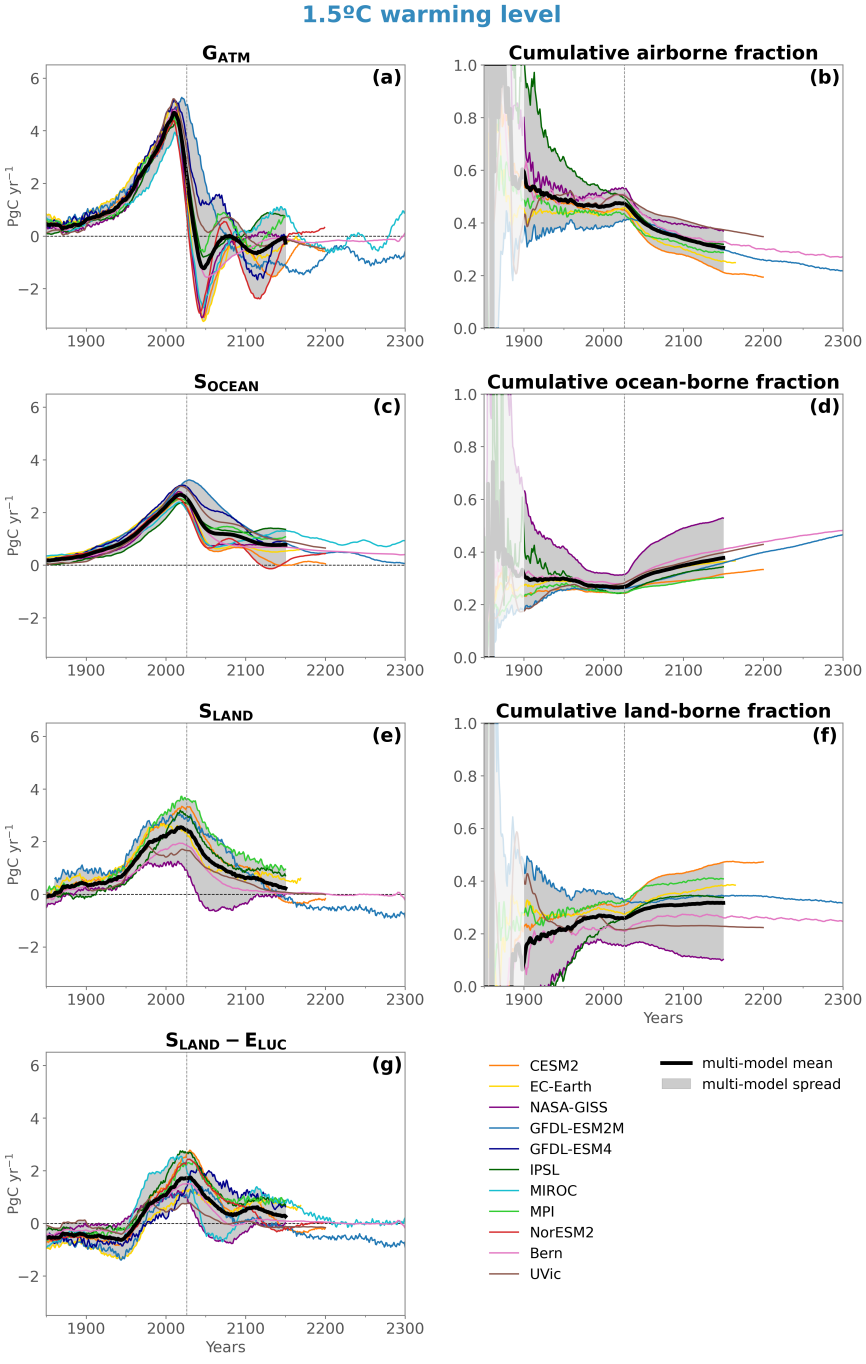

Figure B6. Same as Fig. 6 but for the 1.5 ºC target.

Allen, M. R., Shine, K. P., Fuglestvedt, J. S., Millar, R. J., Cain, M., Frame, D. J., and Macey, A. H.: A solution to the misrepresentations of CO2-equivalent emissions of short-lived climate pollutants under ambitious mitigation, Climate and Atmospheric Science, 1, 16, https://doi.org/10.1038/s41612-018-0026-8, 2018.

https://doi.org/10.5194/egusphere-2024-488
Preprint. Discussion started: 28 February 2024

Arora, V. K., Katavouta, A., Williams, R. G., Jones, C. D., Brovkin, V., Friedlingstein, P., Schwinger, J., Bopp, L., Boucher, O., Cadule, P., Chamberlain, M. A., Christian, J. R., Delire, C., Fisher, R. A., Hajima, T., Ilyina, T., Joetzjer, E., Kawamiya, M., Koven, C. D., Krasting, J. P., Law, R. M., Lawrence, D. M., Lenton, A., Lindsay, K., Pongratz, J., Raddatz, T., Séférian, R., Tachiiri, K., Tjiputra, J. F., Wiltshire, A., Wu, T., and Ziehn, T.: Carbon–concentration and carbon–climate feedbacks in CMIP6 models and their comparison to CMIP5 models, Biogeosciences, 17, 4173–4222, https://doi.org/10.5194/bg-17-4173-2020, publisher: Copernicus GmbH, 2020.

Avrutin, S., Goodwin, P., and Ezard, T. H. G.: Assessing the remaining carbon budget through the lens of policy-driven acidification and temperature targets, Climatic Change, 176, 128, https://doi.org/10.1007/s10584-023-03587-0, 2023.

Battaglia, G. and Joos, F.: Marine N2O Emissions From Nitrification and Denitrification Constrained by Modern Observations and Projected in Multimillennial Global Warming Simulations, Global Biogeochemical Cycles, 32, 92–121, https://doi.org/10.1002/2017GB005671, 2018.

Bonan, D. B., Thompson, A. F., Newsom, E. R., Sun, S., and Rugenstein, M.: Transient and Equilibrium Responses of the Atlantic Overturning Circulation to Warming in Coupled Climate Models: The Role of Temperature and Salinity, Journal of Climate, 35, 5173–5193, https://doi.org/10.1175/JCLI-D-21-0912.1, publisher: American Meteorological Society Section: Journal of Climate, 2022.

Bonnet, R., Boucher, O., Deshayes, J., Gastineau, G., Hourdin, F., Mignot, J., Servonnat, J., and Swingedouw, D.: Presentation and Evaluation of the IPSL-CM6A-LR Ensemble of Extended Historical Simulations, Journal of Advances in Modeling Earth Systems, 13, https://doi.org/10.1029/2021MS002565, 2021.

Boucher, O., Servonnat, J., Albright, A. L., Aumont, O., Balkanski, Y., Bastrikov, V., Bekki, S., Bonnet, R., Bony, S., Bopp, L., Braconnot, P., Brockmann, P., Cadule, P., Caubel, A., Cheruy, F., Codron, F., Cozic, A., Cugnet, D., D'Andrea, F., Davini, P., Lavergne, C., Denvil, S., Deshayes, J., Devilliers, M., Ducharne, A., Dufresne, J., Dupont, E., Éthé, C., Fairhead, L., Falletti, L., Flavoni, S., Foujols, M., Gardoll, S., Gastineau, G., Ghattas, J., Grandpeix, J., Guenet, B., Guez, E., L., Guilyardi, E., Guimberteau, M., Hauglustaine, D., Hourdin, F., Idelkadi, A., Joussaume, S., Kageyama, M., Khodri, M., Krinner, G., Lebas, N., Levavasseur, G., Lévy, C., Li, L., Lott, F., Lurton, T., Luyssaert, S., Madec, G., Madeleine, J., Maignan, F., Marchand, M., Marti, O., Mellul, L., Meurdesoif, Y., Mignot, J., Musat, I., Ottlé, C., Peylin, P., Planton, Y., Polcher, J., Rio, C., Rochetin, N., Rousset, C., Sepulchre, P., Sima, A., Swingedouw, D., Thiéblemont, R., Traore, A. K., Vancoppenolle, M., Vial, J., Vialard, J., Viovy, N., and Vuichard, N.: Presentation and Evaluation of the IPSL-CM6A-LR Climate Model, Journal of Advances in Modeling Earth Systems, 12, https://doi.org/10.1029/2019MS002010, 2020.

Bronselaer, B., Winton, M., Griffies, S. M., Hurlin, W. J., Rodgers, K. B., Sergienko, O. V., Stouffer, R. J., and Russell, J. L.: Change in future climate due to Antarctic meltwater, Nature, 564, 53–58, https://doi.org/10.1038/s41586-018-0712-z, 2018.

Burke, E. J., Ekici, A., Huang, Y., Chadburn, S. E., Huntingford, C., Ciais, P., Friedlingstein, P., Peng, S., and Krinner, G.: Quantifying uncertainties of permafrost carbon–climate feedbacks, Biogeosciences, 14, 3051–3066, https://doi.org/10.5194/bg-14-3051-2017, publisher: Copernicus GmbH, 2017.

Canadell, J., Monteiro, P., Costa, M., Cotrim da Cunha, L., Cox, P., Eliseev, A., Henson, S., Ishii, M., Jaccard, S., Koven, C., Lohila, A., Patra, P., Piao, S., Rogelj, J., Syampungani, S., Zaehle, S., and Zickfeld, K.: Global Carbon and other Biogeochemical Cycles and Feedbacks, in: Climate Change 2021 – The Physical Science Basis: Working Group I Contribution to the Sixth Assessment Report of the Intergovernmental Panel on Climate Change, pp. 673–816, Cambridge University Press, Cambridge, United Kingdom and New York, NY, USA, 1 edn., https://doi.org/10.1017/9781009157896, 2021.

Collins, M., Tett, S. F. B., and Cooper, C.: The internal climate variability of HadCM3, a version of the Hadley Centre coupled model without flux adjustments, Climate Dynamics, 17, 61–81, https://doi.org/10.1007/s003820000094, 2001.

https://doi.org/10.5194/egusphere-2024-488
Preprint. Discussion started: 28 February 2024

Couespel, D. and Tjiputra, J.: What goes in must come out: the oceanic outgassing of anthropogenic carbon, Environmental Research Letters, 19, 014 086, https://doi.org/10.1088/1748-9326/ad16e0, 2024.

Damon Matthews, H., Tokarska, K. B., Rogelj, J., Smith, C. J., MacDougall, A. H., Haustein, K., Mengis, N., Sippel, S., Forster, P. M., and Knutti, R.: An integrated approach to quantifying uncertainties in the remaining carbon budget, Communications Earth & Environment, 2, 7, https://doi.org/10.1038/s43247-020-00064-9, 2021.

Danabasoglu, G., Lamarque, J., Bacmeister, J., Bailey, D. A., DuVivier, A. K., Edwards, J., Emmons, L. K., Fasullo, J., Garcia, R., Gettelman, A., Hannay, C., Holland, M. M., Large, W. G., Lauritzen, P. H., Lawrence, D. M., Lenaerts, J. T. M., Lindsay, K., Lipscomb, W. H., Mills, M. J., Neale, R., Oleson, K. W., Otto-Bliesner, B., Phillips, A. S., Sacks, W., Tilmes, S., Kampenhout, L., Vertenstein, M., Bertini, A., Dennis, J., Deser, C., Fischer, C., Fox-Kemper, B., Kay, J. E., Kinnison, D., Kushner, P. J., Larson, V. E., Long, M. C., Mickelson, S., Moore, J. K., Nienhouse, E., Polvani, L., Rasch, P. J., and Strand, W. G.: The Community Earth System Model Version 2 (CESM2), Journal of Advances in Modeling Earth Systems, 12, https://doi.org/10.1029/2019MS001916, 2020.

Dunne, J. P., John, J. G., Adcroft, A. J., Griffies, S. M., Hallberg, R. W., Shevliakova, E., Stouffer, R. J., Cooke, W., Dunne, K. A., Harrison, M. J., Krasting, J. P., Malyshev, S. L., Milly, P. C. D., Phillipps, P. J., Sentman, L. T., Samuels, B. L., Spelman, M. J., Winton, M., Wittenberg, A. T., and Zadeh, N.: GFDL's ESM2 Global Coupled Climate–Carbon Earth System Models. Part I: Physical Formulation and Baseline Simulation Characteristics, Journal of Climate, 25, 6646–6665, https://doi.org/10.1175/JCLI-D-11-00560.1, 2012.

Dunne, J. P., John, J. G., Shevliakova, E., Stouffer, R. J., Krasting, J. P., Malyshev, S. L., Milly, P. C. D., Sentman, L. T., Adcroft, A. J., Cooke, W., Dunne, K. A., Griffies, S. M., Hallberg, R. W., Harrison, M. J., Levy, H., Wittenberg, A. T., Phillips, P. J., and Zadeh, N.: GFDL's ESM2 Global Coupled Climate–Carbon Earth System Models. Part II: Carbon System Formulation and Baseline Simulation Characteristics*, Journal of Climate, 26, 2247–2267, https://doi.org/10.1175/JCLI-D-12-00150.1, 2013.

Dunne, J. P., Horowitz, L. W., Adcroft, A. J., Ginoux, P., Held, I. M., John, J. G., Krasting, J. P., Malyshev, S., Naik, V., Paulot, F., Shevliakova, E., Stock, C. A., Zadeh, N., Balaji, V., Blanton, C., Dunne, K. A., Dupuis, C., Durachta, J., Dussin, R., Gauthier, P. P. G., Griffies, S. M., Guo, H., Hallberg, R. W., Harrison, M., He, J., Hurlin, W., McHugh, C., Menzel, R., Milly, P. C. D., Nikonov, S., Paynter, D. J., Ploshay, J., Radhakrishnan, A., Rand, K., Reichl, B. G., Robinson, T., Schwarzkopf, D. M., Sentman, L. T., Underwood, S., Vahlenkamp, H., Winton, M., Wittenberg, A. T., Wyman, B., Zeng, Y., and Zhao, M.: The GFDL Earth System Model Version 4.1 (GFDL-ESM 4.1): Overall Coupled Model Description and Simulation Characteristics, Journal of Advances in Modeling Earth Systems, 12, e2019MS002 015, https://doi.org/10.1029/2019MS002015, _eprint: https://onlinelibrary.wiley.com/doi/pdf/10.1029/2019MS002015, 2020.

Döscher, R., Acosta, M., Alessandri, A., Anthoni, P., Arsouze, T., Bergman, T., Bernardello, R., Boussetta, S., Caron, L.-P., Carver, G., Castrillo, M., Catalano, F., Cvijanovic, I., Davini, P., Dekker, E., Doblas-Reyes, F. J., Docquier, D., Echevarria, P., Fladrich, U., Fuentes-Franco, R., Gröger, M., v. Hardenberg, J., Hieronymus, J., Karami, M. P., Keskinen, J.-P., Koenigk, T., Makkonen, R., Massonnet, F., Ménégoz, M., Miller, P. A., Moreno-Chamarro, E., Nieradzik, L., van Noije, T., Nolan, P., O'Donnell, D., Ollinaho, P., van den Oord, G., Ortega, P., Prims, O. T., Ramos, A., Reerink, T., Rousset, C., Ruprich-Robert, Y., Le Sager, P., Schmith, T., Schrödner, R., Serva, F., Sicardi, V., Sloth Madsen, M., Smith, B., Tian, T., Tourigny, E., Uotila, P., Vancoppenolle, M., Wang, S., Wårlind, D., Willén, U., Wyser, K., Yang, S., Yepes-Arbós, X., and Zhang, Q.: The EC-Earth3 Earth system model for the Coupled Model Intercomparison Project 6, Geoscientific Model Development, 15, 2973–3020, https://doi.org/10.5194/gmd-15-2973-2022, publisher: Copernicus GmbH, 2022.

Enting, I. G., Wigley, T. M. L., and Heimann, M.: Future Emissions and Concentrations of Carbon Dioxide: Key Ocean/Atmosphere/Land Analyses, 1994.

Fay, A. R. and McKinley, G. A.: Global open-ocean biomes: mean and temporal variability, Earth System Science Data, 6, 273–284, https://doi.org/10.5194/essd-6-273-2014, publisher: Copernicus GmbH, 2014.

https://doi.org/10.5194/egusphere-2024-488
Preprint. Discussion started: 28 February 2024

Forster, P. M., Smith, C. J., Walsh, T., Lamb, W. F., Lamboll, R., Hauser, M., Ribes, A., Rosen, D., Gillett, N., Palmer, M. D., Rogelj, J., von Schuckmann, K., Seneviratne, S. I., Trewin, B., Zhang, X., Allen, M., Andrew, R., Birt, A., Borger, A., Boyer, T., Broersma, J. A., Cheng, L., Dentener, F., Friedlingstein, P., Gutiérrez, J. M., Gütschow, J., Hall, B., Ishii, M., Jenkins, S., Lan, X., Lee, J.-Y., Morice, C., Kadow, C., Kennedy, J., Killick, R., Minx, J. C., Naik, V., Peters, G. P., Pirani, A., Pongratz, J., Schleussner, C.-F., Szopa, S., Thorne, P., Rohde, R., Rojas Corradi, M., Schumacher, D., Vose, R., Zickfeld, K., Masson-Delmotte, V., and Zhai, P.: Indicators of Global Climate Change 2022: annual update of large-scale indicators of the state of the climate system and human influence, Earth System Science Data, 15, 2295–2327, https://doi.org/10.5194/essd-15-2295-2023, publisher: Copernicus GmbH, 2023.

Friedlingstein, P., O'Sullivan, M., Jones, M. W., Andrew, R. M., Hauck, J., Olsen, A., Peters, G. P., Peters, W., Pongratz, J., Sitch, S., Le Quéré, C., Canadell, J. G., Ciais, P., Jackson, R. B., Alin, S., Aragão, L. E. O. C., Arneth, A., Arora, V., Bates, N. R., Becker, M., Benoit-Cattin, A., Bittig, H. C., Bopp, L., Bultan, S., Chandra, N., Chevallier, F., Chini, L. P., Evans, W., Florentie, L., Forster, P. M., Gasser, T., Gehlen, M., Gilfillan, D., Gkritzalis, T., Gregor, L., Gruber, N., Harris, I., Hartung, K., Haverd, V., Houghton, R. A., Ilyina, T., Jain, A. K., Joetzjer, E., Kadono, K., Kato, E., Kitidis, V., Korsbakken, J. I., Landschützer, P., Lefèvre, N., Lenton, A., Lienert, S., Liu, Z., Lombardozzi, D., Marland, G., Metzl, N., Munro, D. R., Nabel, J. E. M. S., Nakaoka, S.-I., Niwa, Y., O'Brien, K., Ono, T., Palmer, P. I., Pierrot, D., Poulter, B., Resplandy, L., Robertson, E., Rödenbeck, C., Schwinger, J., Séférian, R., Skjelvan, I., Smith, A. J. P., Sutton, A. J., Tanhua, T., Tans, P. P., Tian, H., Tilbrook, B., van der Werf, G., Vuichard, N., Walker, A. P., Wanninkhof, R., Watson, A. J., Willis, D., Wiltshire, A. J., Yuan, W., Yue, X., and Zaehle, S.: Global Carbon Budget 2020, Earth System Science Data, 12, 3269–3340, https://doi.org/10.5194/essd-12-3269-2020, 2020.

Friedlingstein, P., Jones, M. W., O'Sullivan, M., Andrew, R. M., Bakker, D. C. E., Hauck, J., Le Quéré, C., Peters, G. P., Peters, W., Pongratz, J., Sitch, S., Canadell, J. G., Ciais, P., Jackson, R. B., Alin, S. R., Anthoni, P., Bates, N. R., Becker, M., Bellouin, N., Bopp, L., Chau, T. T. T., Chevallier, F., Chini, L. P., Cronin, M., Currie, K. I., Decharme, B., Djeutchouang, L. M., Dou, X., Evans, W., Feely, R. A., Feng, L., Gasser, T., Gilfillan, D., Gkritzalis, T., Grassi, G., Gregor, L., Gruber, N., Gürses, O., Harris, I., Houghton, R. A., Hurtt, G. C., Iida, Y., Ilyina, T., Luijkx, I. T., Jain, A., Jones, S. D., Kato, E., Kennedy, D., Klein Goldewijk, K., Knauer, J., Korsbakken, J. I., Körtzinger, A., Landschützer, P., Lauvset, S. K., Lefèvre, N., Lienert, S., Liu, J., Marland, G., McGuire, P. C., Melton, J. R., Munro, D. R., Nabel, J. E. M. S., Nakaoka, S.-I., Niwa, Y., Ono, T., Pierrot, D., Poulter, B., Rehder, G., Resplandy, L., Robertson, E., Rödenbeck, C., Rosan, T. M., Schwinger, J., Schwingshackl, C., Séférian, R., Sutton, A. J., Sweeney, C., Tanhua, T., Tans, P. P., Tian, H., Tilbrook, B., Tubiello, F., van der Werf, G. R., Vuichard, N., Wada, C., Wanninkhof, R., Watson, A. J., Willis, D., Wiltshire, A. J., Yuan, W., Yue, C., Yue, X., Zaehle, S., and Zeng, J.: Global Carbon Budget 2021, Earth System Science Data, 14, 1917–2005, https://doi.org/10.5194/essd-14-1917-2022, 2022.

Frölicher, T., Terhaar, J., Joos, F., and Silvy, Y.: Protocol for Adaptive Emission Reduction Approach (AERA) simulations, https://doi.org/10.5281/zenodo.6982861, publisher: Zenodo Version Number: v2.0, 2022.

Frölicher, T. L. and Paynter, D. J.: Extending the relationship between global warming and cumulative carbon emissions to multi-millennial timescales, Environmental Research Letters, 10, 075 002, https://doi.org/10.1088/1748-9326/10/7/075002, 2015.

Frölicher, T. L., Winton, M., and Sarmiento, J. L.: Continued global warming after CO2 emissions stoppage, Nature Climate Change, 4, 40–44, https://doi.org/10.1038/nclimate2060, 2014.

Frölicher, T. L., Sarmiento, J. L., Paynter, D. J., Dunne, J. P., Krasting, J. P., and Winton, M.: Dominance of the Southern Ocean in Anthropogenic Carbon and Heat Uptake in CMIP5 Models, Journal of Climate, 28, 862–886, https://doi.org/10.1175/JCLI-D-14-00117.1, 2015.

https://doi.org/10.5194/egusphere-2024-488
Preprint. Discussion started: 28 February 2024

Frölicher, T. L., Aschwanden, M. T., Gruber, N., Jaccard, S. L., Dunne, J. P., and Paynter, D.: Contrasting Upper and Deep Ocean Oxygen Response to Protracted Global Warming, Global Biogeochemical Cycles, 34, https://doi.org/10.1029/2020GB006601, 2020.

Gasser, T., Kechiar, M., Ciais, P., Burke, E. J., Kleinen, T., Zhu, D., Huang, Y., Ekici, A., and Obersteiner, M.: Path-dependent reductions in CO2 emission budgets caused by permafrost carbon release, Nature Geoscience, 11, 830–835, https://doi.org/10.1038/s41561-018-0227-0, number: 11 Publisher: Nature Publishing Group, 2018.

Goodwin, P., Brown, S., Haigh, I. D., Nicholls, R. J., and Matter, J. M.: Adjusting Mitigation Pathways to Stabilize Climate at 1.5°C and 2.0°C Rise in Global Temperatures to Year 2300, Earth's Future, 6, 601–615, https://doi.org/10.1002/2017EF000732, _eprint: https://onlinelibrary.wiley.com/doi/pdf/10.1002/2017EF000732, 2018a.

Goodwin, P., Katavouta, A., Roussenov, V. M., Foster, G. L., Rohling, E. J., and Williams, R. G.: Pathways to 1.5 °C and 2 °C warming based on observational and geological constraints, Nature Geoscience, 11, 102–107, https://doi.org/10.1038/s41561-017-0054-8, number: 2 Publisher: Nature Publishing Group, 2018b.

Hajima, T., Watanabe, M., Yamamoto, A., Tatebe, H., Noguchi, M. A., Abe, M., Ohgaito, R., Ito, A., Yamazaki, D., Okajima, H., Ito, A., Takata, K., Ogochi, K., Watanabe, S., and Kawamiya, M.: Development of the MIROC-ES2L Earth system model and the evaluation of biogeochemical processes and feedbacks, Geoscientific Model Development, 13, 2197–2244, https://doi.org/10.5194/gmd-13-2197-2020, publisher: Copernicus GmbH, 2020.

Haustein, K., Allen, M. R., Forster, P. M., Otto, F. E. L., Mitchell, D. M., Matthews, H. D., and Frame, D. J.: A real-time Global Warming Index, Scientific Reports, 7, 15 417, https://doi.org/10.1038/s41598-017-14828-5, 2017.

Hoffman, F. M., Randerson, J. T., Arora, V. K., Bao, Q., Cadule, P., Ji, D., Jones, C. D., Kawamiya, M., Khatiwala, S., Lindsay, K., Obata, A., Shevliakova, E., Six, K. D., Tjiputra, J. F., Volodin, E. M., and Wu, T.: Causes and implications of persistent atmospheric carbon dioxide biases in Earth System Models, Journal of Geophysical Research: Biogeosciences, 119, 141–162, https://doi.org/10.1002/2013JG002381, 2014.

IPCC: Summary for Policymakers, in: Global warming of 1.5°C. An IPCC Special Report on the impacts of global warming of 1.5°C above pre-industrial levels and related global greenhouse gas emission pathways, in the context of strengthening the global response to the threat of climate change, sustainable development, and efforts to eradicate poverty, http://www.ipcc.ch/report/sr15/, oCLC: 1056192590, 2018.

IPCC: Technical Summary, in: Climate Change 2021 – The Physical Science Basis: Working Group I Contribution to the Sixth Assessment Report of the Intergovernmental Panel on Climate Change, Cambridge University Press, 1 edn., https://doi.org/10.1017/9781009157896, 2021.

IPCC: Summary for Policymakers, in: Climate Change 2022: Impacts, Adaptation, and Vulnerability. Contribution of Working Group II to the Sixth Assessment Report of the Intergovernmental Panel on Climate Change, Cambridge University Press, 2022.

Ito, G., Romanou, A., Kiang, N. Y., Faluvegi, G., Aleinov, I., Ruedy, R., Russell, G., Lerner, P., Kelley, M., and Lo, K.: Global Carbon Cycle and Climate Feedbacks in the NASA GISS ModelE2.1, Journal of Advances in Modeling Earth Systems, 12, e2019MS002 030, https://doi.org/10.1029/2019MS002030, _eprint: https://onlinelibrary.wiley.com/doi/pdf/10.1029/2019MS002030, 2020.

Jenkins, S., Millar, R. J., Leach, N., and Allen, M. R.: Framing Climate Goals in Terms of Cumulative CO2-Forcing-Equivalent Emissions, Geophysical Research Letters, 45, 2795–2804, https://doi.org/10.1002/2017GL076173, 2018.

Jenkins, S., Cain, M., Friedlingstein, P., Gillett, N., Walsh, T., and Allen, M. R.: Quantifying non-CO2 contributions to remaining carbon budgets, npj Climate and Atmospheric Science, 4, 1–10, https://doi.org/10.1038/s41612-021-00203-9, number: 1 Publisher: Nature Publishing Group, 2021.

https://doi.org/10.5194/egusphere-2024-488
Preprint. Discussion started: 28 February 2024

Jenkins, S., Povey, A., Gettelman, A., Grainger, R., Stier, P., and Allen, M.: Is Anthropogenic Global Warming Accelerating?, Journal of Climate, 35, 7873–7890, https://doi.org/10.1175/JCLI-D-22-0081.1, publisher: American Meteorological Society Section: Journal of Climate, 2022a.

Jenkins, S., Sanderson, B., Peters, G., Frölicher, T. L., Friedlingstein, P., and Allen, M.: The Multi-Decadal Response to Net Zero CO2 Emissions and Implications for Emissions Policy, Geophysical Research Letters, 49, https://doi.org/10.1029/2022GL101047, 2022b.

Kelley, M., Schmidt, G. A., Nazarenko, L. S., Bauer, S. E., Ruedy, R., Russell, G. L., Ackerman, A. S., Aleinov, I., Bauer, M., Bleck, R., Canuto, V., Cesana, G., Cheng, Y., Clune, T. L., Cook, B. I., Cruz, C. A., Del Genio, A. D., Elsaesser, G. S., Faluvegi, G., Kiang, N. Y., Kim, D., Lacis, A. A., Leboissetier, A., LeGrande, A. N., Lo, K. K., Marshall, J., Matthews, E. E., McDermid, S., Mezuman, K., Miller, R. L., Murray, L. T., Oinas, V., Orbe, C., García-Pando, C. P., Perlwitz, J. P., Puma, M. J., Rind, D., Romanou, A., Shindell, D. T., Sun, S., Tausnev, N., Tsigaridis, K., Tselioudis, G., Weng, E., Wu, J., and Yao, M.-S.: GISS-E2.1: Configurations and Climatology, Journal of Advances in Modeling Earth Systems, 12, e2019MS002 025, https://doi.org/10.1029/2019MS002025, _eprint: https://onlinelibrary.wiley.com/doi/pdf/10.1029/2019MS002025, 2020.

King, A. D., Sniderman, J. M. K., Dittus, A. J., Brown, J. R., Hawkins, E., and Ziehn, T.: Studying climate stabilization at Paris Agreement levels, Nature Climate Change, 11, 1010–1013, https://doi.org/10.1038/s41558-021-01225-0, 2021.

Koven, C. D., Arora, V. K., Cadule, P., Fisher, R. A., Jones, C. D., Lawrence, D. M., Lewis, J., Lindsay, K., Mathesius, S., Meinshausen, M., Mills, M., Nicholls, Z., Sanderson, B. M., Séférian, R., Swart, N. C., Wieder, W. R., and Zickfeld, K.: Multi-century dynamics of the climate and carbon cycle under both high and net negative emissions scenarios, Earth System Dynamics, 13, 885–909, https://doi.org/10.5194/esd-13-885-2022, 2022.

Lago, V. and England, M. H.: Projected Slowdown of Antarctic Bottom Water Formation in Response to Amplified Meltwater Contributions, Journal of Climate, 32, 6319–6335, https://doi.org/10.1175/JCLI-D-18-0622.1, 2019.

Lan, X., Tans, P., Thoning, K., and NOAA Global Monitoring Laboratory: Trends in globally-averaged CO2 determined from NOAA Global Monitoring Laboratory measurements., https://doi.org/10.15138/9N0H-ZH07, 2023.

Lawrence, D. M., Hurtt, G. C., Arneth, A., Brovkin, V., Calvin, K. V., Jones, A. D., Jones, C. D., Lawrence, P. J., de Noblet-Ducoudré, N., Pongratz, J., Seneviratne, S. I., and Shevliakova, E.: The Land Use Model Intercomparison Project (LUMIP) contribution to CMIP6: rationale and experimental design, Geoscientific Model Development, 9, 2973–2998, https://doi.org/10.5194/gmd-9-2973-2016, 2016.

Le Quéré, C., Peters, G. P., Friedlingstein, P., Andrew, R. M., Canadell, J. G., Davis, S. J., Jackson, R. B., and Jones, M. W.: Fossil CO2 emissions in the post-COVID-19 era, Nature Climate Change, 11, 197–199, https://doi.org/10.1038/s41558-021-01001-0, number: 3 Publisher: Nature Publishing Group, 2021.

Leach, N. J., Jenkins, S., Nicholls, Z., Smith, C. J., Lynch, J., Cain, M., Walsh, T., Wu, B., Tsutsui, J., and Allen, M. R.: FaIRv2.0.0: a generalized impulse response model for climate uncertainty and future scenario exploration, Geoscientific Model Development, 14, 3007–3036, https://doi.org/10.5194/gmd-14-3007-2021, publisher: Copernicus GmbH, 2021.

Lehner, F., Deser, C., Maher, N., Marotzke, J., Fischer, E. M., Brunner, L., Knutti, R., and Hawkins, E.: Partitioning climate projection uncertainty with multiple large ensembles and CMIP5/6, Earth System Dynamics, 11, 491–508, https://doi.org/10.5194/esd-11-491-2020, 2020.

Lerner, P., Romanou, A., Nicholson, D., Kelley, M., Ruedy, R., and Russell, G.: The sensitivity of the equatorial pacific ODZ to particulate organic matter remineralization in a climate model under pre-industrial conditions, Ocean Modelling, 188, 102 303, https://doi.org/10.1016/j.ocemod.2023.102303, 2024.

https://doi.org/10.5194/egusphere-2024-488
Preprint. Discussion started: 28 February 2024

Li, Q., England, M. H., Hogg, A. M., Rintoul, S. R., and Morrison, A. K.: Abyssal ocean overturning slowdown and warming driven by Antarctic meltwater, Nature, 615, 841–847, https://doi.org/10.1038/s41586-023-05762-w, number: 7954 Publisher: Nature Publishing Group, 2023.

Liddicoat, S. K., Wiltshire, A. J., Jones, C. D., Arora, V. K., Brovkin, V., Cadule, P., Hajima, T., Lawrence, D. M., Pongratz, J., Schwinger, J., Séférian, R., Tjiputra, J. F., and Ziehn, T.: Compatible Fossil Fuel CO2 Emissions in the CMIP6 Earth System Models' Historical and Shared Socioeconomic Pathway Experiments of the Twenty-First Century, Journal of Climate, 34, 2853–2875, https://doi.org/10.1175/JCLI-D-19-0991.1, 2021.

Lowe, J. A. and Bernie, D.: The impact of Earth system feedbacks on carbon budgets and climate response, Philosophical Transactions of the Royal Society A: Mathematical, Physical and Engineering Sciences, 376, 20170 263, https://doi.org/10.1098/rsta.2017.0263, publisher: Royal Society, 2018.

MacDougall, A. H.: Estimated effect of the permafrost carbon feedback on the zero emissions commitment to climate change, Biogeosciences, 18, 4937–4952, https://doi.org/10.5194/bg-18-4937-2021, publisher: Copernicus GmbH, 2021.

MacDougall, A. H. and Friedlingstein, P.: The Origin and Limits of the Near Proportionality between Climate Warming and Cumulative CO2 Emissions, Journal of Climate, 28, 4217–4230, https://doi.org/10.1175/JCLI-D-14-00036.1, publisher: American Meteorological Society Section: Journal of Climate, 2015.

MacDougall, A. H., Zickfeld, K., Knutti, R., and Matthews, H. D.: Sensitivity of carbon budgets to permafrost carbon feedbacks and non-CO2 forcings, Environmental Research Letters, 10, 125 003, https://doi.org/10.1088/1748-9326/10/12/125003, publisher: IOP Publishing, 2015.

MacDougall, A. H., Frölicher, T. L., Jones, C. D., Rogelj, J., Matthews, H. D., Zickfeld, K., Arora, V. K., Barrett, N. J., Brovkin, V., Burger, F. A., Eby, M., Eliseev, A. V., Hajima, T., Holden, P. B., Jeltsch-Thömmes, A., Koven, C., Mengis, N., Menviel, L., Michou, M., Mokhov, I. I., Oka, A., Schwinger, J., Séférian, R., Shaffer, G., Sokolov, A., Tachiiri, K., Tjiputra, J., Wiltshire, A., and Ziehn, T.: Is there warming in the pipeline? A multi-model analysis of the Zero Emissions Commitment from CO2, Biogeosciences, 17, 2987–3016, https://doi.org/10.5194/bg-17-2987-2020, 2020.

Manabe, S. and Stouffer, R. J.: Multiple-Century Response of a Coupled Ocean-Atmosphere Model to an Increase of Atmospheric Carbon Dioxide, Journal of Climate, 7, 5–23, https://doi.org/10.1175/1520-0442(1994)007<0005:MCROAC>2.0.CO;2, publisher: American Meteorological Society Section: Journal of Climate, 1994.

Matthews, H. D. and Caldeira, K.: Stabilizing climate requires near-zero emissions, Geophysical Research Letters, 35, https://doi.org/10.1029/2007GL032388, _eprint: https://onlinelibrary.wiley.com/doi/pdf/10.1029/2007GL032388, 2008.

Matthews, H. D., Gillett, N. P., Stott, P. A., and Zickfeld, K.: The proportionality of global warming to cumulative carbon emissions, Nature, 459, 829–832, https://doi.org/10.1038/nature08047, number: 7248 Publisher: Nature Publishing Group, 2009.

Matthews, H. D., Landry, J.-S., Partanen, A.-I., Allen, M., Eby, M., Forster, P. M., Friedlingstein, P., and Zickfeld, K.: Estimating Carbon Budgets for Ambitious Climate Targets, Current Climate Change Reports, 3, 69–77, https://doi.org/10.1007/s40641-017-0055-0, 2017.

Mauritsen, T., Bader, J., Becker, T., Behrens, J., Bittner, M., Brokopf, R., Brovkin, V., Claussen, M., Crueger, T., Esch, M., Fast, I., Fiedler, S., Fläschner, D., Gayler, V., Giorgetta, M., Goll, D. S., Haak, H., Hagemann, S., Hedemann, C., Hohenegger, C., Ilyina, T., Jahns, T., Jimenéz-de-la-Cuesta, D., Jungclaus, J., Kleinen, T., Kloster, S., Kracher, D., Kinne, S., Kleberg, D., Lasslop, G., Kornblueh, L., Marotzke, J., Matei, D., Meraner, K., Mikolajewicz, U., Modali, K., Möbis, B., Müller, W. A., Nabel, J. E. M. S., Nam, C. C. W., Notz, D., Nyawira, S., Paulsen, H., Peters, K., Pincus, R., Pohlmann, H., Pongratz, J., Popp, M., Raddatz, T. J., Rast, S., Redler, R., Reick, C. H., Rohrschneider, T., Schemann, V., Schmidt, H., Schnur, R., Schulzweida, U., Six, K. D., Stein, L., Stemmler, I., Stevens, B., Von Storch,

https://doi.org/10.5194/egusphere-2024-488
Preprint. Discussion started: 28 February 2024

J., Tian, F., Voigt, A., Vrese, P., Wieners, K., Wilkenskjeld, S., Winkler, A., and Roeckner, E.: Developments in the MPI-M Earth System Model version 1.2 (MPI-ESM1.2) and Its Response to Increasing CO_2, Journal of Advances in Modeling Earth Systems, 11, 998–1038, https://doi.org/10.1029/2018MS001400, 2019.

Meehl, G. A., Senior, C. A., Eyring, V., Flato, G., Lamarque, J.-F., Stouffer, R. J., Taylor, K. E., and Schlund, M.: Context for interpreting equilibrium climate sensitivity and transient climate response from the CMIP6 Earth system models, Science Advances, 6, eaba1981, https://doi.org/10.1126/sciadv.aba1981, 2020.

Meinshausen, M., Meinshausen, N., Hare, W., Raper, S. C. B., Frieler, K., Knutti, R., Frame, D. J., and Allen, M. R.: Greenhouse-gas emission targets for limiting global warming to 2 °C, Nature, 458, 1158–1162, https://doi.org/10.1038/nature08017, number: 7242 Publisher: Nature Publishing Group, 2009.

Meinshausen, M., Nicholls, Z. R. J., Lewis, J., Gidden, M. J., Vogel, E., Freund, M., Beyerle, U., Gessner, C., Nauels, A., Bauer, N., Canadell, J. G., Daniel, J. S., John, A., Krummel, P. B., Luderer, G., Meinshausen, N., Montzka, S. A., Rayner, P. J., Reimann, S., Smith, S. J., van den Berg, M., Velders, G. J. M., Vollmer, M. K., and Wang, R. H. J.: The shared socio-economic pathway (SSP) greenhouse gas concentrations and their extensions to 2500, Geoscientific Model Development, 13, 3571–3605, https://doi.org/10.5194/gmd-13-3571-2020, publisher: Copernicus GmbH, 2020.

Mengis, N. and Matthews, H. D.: Non-CO2 forcing changes will likely decrease the remaining carbon budget for 1.5 °C, npj Climate and Atmospheric Science, 3, 1–7, https://doi.org/10.1038/s41612-020-0123-3, number: 1 Publisher: Nature Publishing Group, 2020.

Mengis, N., Partanen, A.-I., Jalbert, J., and Matthews, H. D.: 1.5 °C carbon budget dependent on carbon cycle uncertainty and future non-CO2 forcing, Scientific Reports, 8, 5831, https://doi.org/10.1038/s41598-018-24241-1, 2018.

Mengis, N., Keller, D. P., MacDougall, A. H., Eby, M., Wright, N., Meissner, K. J., Oschlies, A., Schmittner, A., MacIsaac, A. J., Matthews, H. D., and Zickfeld, K.: Evaluation of the University of Victoria Earth System Climate Model version 2.10 (UVic ESCM 2.10), Geoscientific Model Development, 13, 4183–4204, https://doi.org/10.5194/gmd-13-4183-2020, publisher: Copernicus GmbH, 2020.

Mikaloff Fletcher, S. E., Gruber, N., Jacobson, A. R., Doney, S. C., Dutkiewicz, S., Gerber, M., Follows, M., Joos, F., Lindsay, K., Menemenlis, D., Mouchet, A., Müller, S. A., and Sarmiento, J. L.: Inverse estimates of anthropogenic CO2 uptake, transport, and storage by the ocean, Global Biogeochemical Cycles, 20, 2005GB002 530, https://doi.org/10.1029/2005GB002530, 2006.

Millar, R. J. and Friedlingstein, P.: The utility of the historical record for assessing the transient climate response to cumulative emissions, Philosophical Transactions of the Royal Society A: Mathematical, Physical and Engineering Sciences, 376, 20160 449, https://doi.org/10.1098/rsta.2016.0449, 2018.

Millar, R. J., Fuglestvedt, J. S., Friedlingstein, P., Rogelj, J., Grubb, M. J., Matthews, H. D., Skeie, R. B., Forster, P. M., Frame, D. J., and Allen, M. R.: Emission budgets and pathways consistent with limiting warming to 1.5 °C, Nature Geoscience, 10, 741–747, https://doi.org/10.1038/ngeo3031, number: 10 Publisher: Nature Publishing Group, 2017.

Miller, R. L., Schmidt, G. A., Nazarenko, L. S., Bauer, S. E., Kelley, M., Ruedy, R., Russell, G. L., Ackerman, A. S., Aleinov, I., Bauer, M., Bleck, R., Canuto, V., Cesana, G., Cheng, Y., Clune, T. L., Cook, B. I., Cruz, C. A., Del Genio, A. D., Elsaesser, G. S., Faluvegi, G., Kiang, N. Y., Kim, D., Lacis, A. A., Leboissetier, A., LeGrande, A. N., Lo, K. K., Marshall, J., Matthews, E. E., McDermid, S., Mezuman, K., Murray, L. T., Oinas, V., Orbe, C., Pérez García-Pando, C., Perlwitz, J. P., Puma, M. J., Rind, D., Romanou, A., Shindell, D. T., Sun, S., Tausnev, N., Tsigaridis, K., Tselioudis, G., Weng, E., Wu, J., and Yao, M.: CMIP6 Historical Simulations (1850–2014) With GISS-E2.1, Journal of Advances in Modeling Earth Systems, 13, e2019MS002 034, https://doi.org/10.1029/2019MS002034, 2021.

Müller, J. and Joos, F.: Committed and projected future changes in global peatlands – continued transient model simulations since the Last Glacial Maximum, Biogeosciences, 18, 3657–3687, https://doi.org/10.5194/bg-18-3657-2021, publisher: Copernicus GmbH, 2021.

https://doi.org/10.5194/egusphere-2024-488
Preprint. Discussion started: 28 February 2024

Nicholls, Z. R. J., Gieseke, R., Lewis, J., Nauels, A., and Meinshausen, M.: Implications of non-linearities between cumulative CO2 emissions and CO2-induced warming for assessing the remaining carbon budget, Environmental Research Letters, 15, 074 017, https://doi.org/10.1088/1748-9326/ab83af, publisher: IOP Publishing, 2020.

O'Neill, B. C., Tebaldi, C., Vuuren, D. P. v., Eyring, V., Friedlingstein, P., Hurtt, G., Knutti, R., Kriegler, E., Lamarque, J.-F., Lowe, J., Meehl, G. A., Moss, R., Riahi, K., and Sanderson, B. M.: The Scenario Model Intercomparison Project (ScenarioMIP) for CMIP6, Geoscientific Model Development, 9, 3461–3482, https://doi.org/https://doi.org/10.5194/gmd-9-3461-2016, 2016.

Otto, F. E. L., Frame, D. J., Otto, A., and Allen, M. R.: Embracing uncertainty in climate change policy, Nature Climate Change, 5, 917–920, https://doi.org/10.1038/nclimate2716, number: 10 Publisher: Nature Publishing Group, 2015.

Palazzo Corner, S., Siegert, M., Ceppi, P., Fox-Kemper, B., Frölicher, T. L., Gallego-Sala, A., Haigh, J., Hegerl, G. C., Jones, C. D., Knutti, R., Koven, C. D., MacDougall, A. H., Meinshausen, M., Nicholls, Z., Sallée, J. B., Sanderson, B. M., Séférian, R., Turetsky, M., Williams, R. G., Zaehle, S., and Rogelj, J.: The zero emissions commitment and climate stabilisation, Frontiers in Science, 0, https://doi.org/10.3389/fsci.2023.1170744, publisher: Frontiers, 2023.

Ritz, S. P., Stocker, T. F., and Joos, F.: A Coupled Dynamical Ocean–Energy Balance Atmosphere Model for Paleoclimate Studies, Journal of Climate, 24, 349–375, https://doi.org/10.1175/2010JCLI3351.1, publisher: American Meteorological Society Section: Journal of Climate, 2011.

Rockström, J., Steffen, W., Noone, K., Persson, , Chapin, F. S., Lambin, E. F., Lenton, T. M., Scheffer, M., Folke, C., Schellnhuber, H. J., Nykvist, B., De Wit, C. A., Hughes, T., Van Der Leeuw, S., Rodhe, H., Sörlin, S., Snyder, P. K., Costanza, R., Svedin, U., Falkenmark, M., Karlberg, L., Corell, R. W., Fabry, V. J., Hansen, J., Walker, B., Liverman, D., Richardson, K., Crutzen, P., and Foley, J. A.: A safe operating space for humanity, Nature, 461, 472–475, https://doi.org/10.1038/461472a, 2009.

Rodgers, K. B., Schlunegger, S., Slater, R. D., Ishii, M., Frölicher, T. L., Toyama, K., Plancherel, Y., Aumont, O., and Fassbender, A. J.: Reemergence of Anthropogenic Carbon Into the Ocean's Mixed Layer Strongly Amplifies Transient Climate Sensitivity, Geophysical Research Letters, 47, e2020GL089 275, https://doi.org/10.1029/2020GL089275, _eprint: https://onlinelibrary.wiley.com/doi/pdf/10.1029/2020GL089275, 2020.

Rogelj, J., Schaeffer, M., Friedlingstein, P., Gillett, N. P., van Vuuren, D. P., Riahi, K., Allen, M., and Knutti, R.: Differences between carbon budget estimates unravelled, Nature Climate Change, 6, 245–252, https://doi.org/10.1038/nclimate2868, number: 3 Publisher: Nature Publishing Group, 2016.

Rogelj, J., Forster, P. M., Kriegler, E., Smith, C. J., and Séférian, R.: Estimating and tracking the remaining carbon budget for stringent climate targets, Nature, 571, 335–342, https://doi.org/10.1038/s41586-019-1368-z, 2019.

Roy, T., Bopp, L., Gehlen, M., Schneider, B., Cadule, P., Frölicher, T. L., Segschneider, J., Tjiputra, J., Heinze, C., and Joos, F.: Regional Impacts of Climate Change and Atmospheric CO2 on Future Ocean Carbon Uptake: A Multimodel Linear Feedback Analysis, Journal of Climate, 24, 2300–2318, https://doi.org/10.1175/2010JCLI3787.1, 2011.

Sanderson, B. M., Booth, B. B. B., Dunne, J., Eyring, V., Fisher, R. A., Friedlingstein, P., Gidden, M. J., Hajima, T., Jones, C. D., Jones, C., King, A., Koven, C. D., Lawrence, D. M., Lowe, J., Mengis, N., Peters, G. P., Rogelj, J., Smith, C., Snyder, A. C., Simpson, I. R., Swann, A. L. S., Tebaldi, C., Ilyina, T., Schleussner, C.-F., Seferian, R., Samset, B. H., van Vuuren, D., and Zaehle, S.: The need for carbon emissions-driven climate projections in CMIP7, EGUsphere, pp. 1–51, https://doi.org/10.5194/egusphere-2023-2127, publisher: Copernicus GmbH, 2023.

Schwinger, J., Asaadi, A., Goris, N., and Lee, H.: Possibility for strong northern hemisphere high-latitude cooling under negative emissions, Nature Communications, 13, 1095, https://doi.org/10.1038/s41467-022-28573-5, number: 1 Publisher: Nature Publishing Group, 2022.

https://doi.org/10.5194/egusphere-2024-488
Preprint. Discussion started: 28 February 2024

Seland, , Bentsen, M., Olivié, D., Toniazzo, T., Gjermundsen, A., Graff, L. S., Debernard, J. B., Gupta, A. K., He, Y.-C., Kirkevåg, A., Schwinger, J., Tjiputra, J., Aas, K. S., Bethke, I., Fan, Y., Griesfeller, J., Grini, A., Guo, C., Ilicak, M., Karset, I. H. H., Landgren, O., Liakka, J., Moseid, K. O., Nummelin, A., Spensberger, C., Tang, H., Zhang, Z., Heinze, C., Iversen, T., and Schulz, M.: Overview of the Norwegian Earth System Model (NorESM2) and key climate response of CMIP6 DECK, historical, and scenario simulations, Geoscientific Model Development, 13, 6165–6200, https://doi.org/10.5194/gmd-13-6165-2020, publisher: Copernicus GmbH, 2020.

Seneviratne, S. I., Donat, M. G., Pitman, A. J., Knutti, R., and Wilby, R. L.: Allowable CO2 emissions based on regional and impact-related climate targets, Nature, 529, 477–483, https://doi.org/10.1038/nature16542, number: 7587 Publisher: Nature Publishing Group, 2016.

Siegenthaler, U. and Joos, F.: Use of a simple model for studying oceanic tracer distributions and the global carbon cycle, Tellus B, 44, 186–207, https://doi.org/10.1034/j.1600-0889.1992.t01-2-00003.x, _eprint: https://onlinelibrary.wiley.com/doi/pdf/10.1034/j.1600-0889.1992.t01-2-00003.x, 1992.

Sigmond, M., Fyfe, J. C., Saenko, O. A., and Swart, N. C.: Ongoing AMOC and related sea-level and temperature changes after achieving the Paris targets, Nature Climate Change, 10, 672–677, https://doi.org/10.1038/s41558-020-0786-0, 2020.

Silvy, Y., Frölicher, T., Terhaar, J., Joos, F., Burger, F., Lacroix, F., Allen, M., Bernadello, R., bopp, l., Brovkin, V., Buzan, J., CADULE, P., Dix, M., Dunne, J., Friedlingstein, P., Georgievski, G., Hajima, T., Jenkins, S., Kawamiya, M., Kiang, N. Y., Lapin, V., Donghyun, L., Lerner, P., Mengis, N., Monteiro, E., Paynter, D., Peters, G. P., Romanou, A., Schwinger, J., Sparrow, S., Stofferahn, E., Tjiputra, J., Tourigny, E., and Ziehn, T.: Model data for "AERA-MIP: Emission pathways, remaining budgets and carbon cycle dynamics compatible with 1.5 ºC and 2 ºC global warming stabilization", https://doi.org/10.5281/ZENODO.10715168, 2024.

Smith, C.: Effective Radiative Forcing Time Series from the Shared Socioeconomic Pathways, https://doi.org/10.5281/zenodo.3973015, 2020.

Smith, C., Walsh, T., Borger, A., Forster, P., Gillett, N., Hauser, M., Lamb, W., Lamboll, R., Palmer, M., Ribes, A., Schumacher, D., Seneviratne, S., Trewin, B., and Schuckmann, K. v.: Indicators of Global Climate Change 2022, https://doi.org/10.5281/zenodo.8000192, 2023.

Smith, M. A., Cain, M., and Allen, M. R.: Further improvement of warming-equivalent emissions calculation, npj Climate and Atmospheric Science, 4, 1–3, https://doi.org/10.1038/s41612-021-00169-8, number: 1 Publisher: Nature Publishing Group, 2021.

Sparrow, S., Millar, R. J., Yamazaki, K., Massey, N., Povey, A. C., Bowery, A., Grainger, R. G., Wallom, D., and Allen, M.: Finding Ocean States That Are Consistent with Observations from a Perturbed Physics Parameter Ensemble, Journal of Climate, 31, 4639–4656, https://doi.org/10.1175/JCLI-D-17-0514.1, publisher: American Meteorological Society Section: Journal of Climate, 2018.

Steinacher, M. and Joos, F.: Transient Earth system responses to cumulative carbon dioxide emissions: linearities, uncertainties, and probabilities in an observation-constrained model ensemble, Biogeosciences, 13, 1071–1103, https://doi.org/10.5194/bg-13-1071-2016, publisher: Copernicus GmbH, 2016.

Steinacher, M., Joos, F., and Stocker, T. F.: Allowable carbon emissions lowered by multiple climate targets, Nature, 499, 197–201, https://doi.org/10.1038/nature12269, 2013.

Stocker, B. D., Roth, R., Joos, F., Spahni, R., Steinacher, M., Zaehle, S., Bouwman, L., Xu-Ri, and Prentice, I. C.: Multiple greenhouse-gas feedbacks from the land biosphere under future climate change scenarios, Nature Climate Change, 3, 666–672, https://doi.org/10.1038/nclimate1864, 2013.

Séférian, R., Berthet, S., Yool, A., Palmiéri, J., Bopp, L., Tagliabue, A., Kwiatkowski, L., Aumont, O., Christian, J., Dunne, J., Gehlen, M., Ilyina, T., John, J. G., Li, H., Long, M. C., Luo, J. Y., Nakano, H., Romanou, A., Schwinger, J., Stock, C., Santana-Falcón, Y., Takano, Y., Tjiputra, J., Tsujino, H., Watanabe, M., Wu, T., Wu, F., and Yamamoto, A.: Tracking Improvement in Simulated Marine Biogeochemistry Between CMIP5 and CMIP6, Current Climate Change Reports, 6, 95–119, https://doi.org/10.1007/s40641-020-00160-0, 2020.

https://doi.org/10.5194/egusphere-2024-488
Preprint. Discussion started: 28 February 2024

Tebaldi, C., Debeire, K., Eyring, V., Fischer, E., Fyfe, J., Friedlingstein, P., Knutti, R., Lowe, J., O'Neill, B., Sanderson, B., van Vuuren, D., Riahi, K., Meinshausen, M., Nicholls, Z., Tokarska, K. B., Hurtt, G., Kriegler, E., Lamarque, J.-F., Meehl, G., Moss, R., Bauer, S. E., Boucher, O., Brovkin, V., Byun, Y.-H., Dix, M., Gualdi, S., Guo, H., John, J. G., Kharin, S., Kim, Y., Koshiro, T., Ma, L., Olivié, D., Panickal, S., Qiao, F., Rong, X., Rosenbloom, N., Schupfner, M., Séférian, R., Sellar, A., Semmler, T., Shi, X., Song, Z., Steger, C., Stouffer, R., Swart, N., Tachiiri, K., Tang, Q., Tatebe, H., Voldoire, A., Volodin, E., Wyser, K., Xin, X., Yang, S., Yu, Y., and Ziehn, T.: Climate model projections from the Scenario Model Intercomparison Project (ScenarioMIP) of CMIP6, Earth System Dynamics, 12, 253–293, https://doi.org/10.5194/esd-12-253-2021, publisher: Copernicus GmbH, 2021.

Terhaar, J., Tanhua, T., Stöven, T., Orr, J. C., and Bopp, L.: Evaluation of Data-Based Estimates of Anthropogenic Carbon in the Arctic Ocean, Journal of Geophysical Research: Oceans, 125, e2020JC016 124, https://doi.org/10.1029/2020JC016124, _eprint: https://onlinelibrary.wiley.com/doi/pdf/10.1029/2020JC016124, 2020.

Terhaar, J., Frölicher, T. L., and Joos, F.: Southern Ocean anthropogenic carbon sink constrained by sea surface salinity, Science Advances, 7, eabd5964, https://doi.org/10.1126/sciadv.abd5964, 2021.

Terhaar, J., Frölicher, T. L., Aschwanden, M. T., Friedlingstein, P., and Joos, F.: Adaptive emission reduction approach to reach any global warming target, Nature Climate Change, 12, 1136–1142, https://doi.org/10.1038/s41558-022-01537-9, number: 12 Publisher: Nature Publishing Group, 2022a.

Terhaar, J., Frölicher, T. L., and Joos, F.: Observation-constrained estimates of the global ocean carbon sink from Earth system models, Biogeosciences, 19, 4431–4457, https://doi.org/10.5194/bg-19-4431-2022, publisher: Copernicus GmbH, 2022b.

Terhaar, J., Frölicher, T. L., and Joos, F.: Ocean acidification in emission-driven temperature stabilization scenarios: the role of TCRE and non-CO2 greenhouse gases, Environmental Research Letters, 18, 024 033, https://doi.org/10.1088/1748-9326/acaf91, 2023.

Tjiputra, J. F., Assmann, K., and Heinze, C.: Anthropogenic carbon dynamics in the changing ocean, Ocean Science, 6, 605–614, https://doi.org/10.5194/os-6-605-2010, 2010.

Tjiputra, J. F., Schwinger, J., Bentsen, M., Morée, A. L., Gao, S., Bethke, I., Heinze, C., Goris, N., Gupta, A., He, Y.-C., Olivié, D., Seland, , and Schulz, M.: Ocean biogeochemistry in the Norwegian Earth System Model version 2 (NorESM2), Geoscientific Model Development, 13, 2393–2431, https://doi.org/10.5194/gmd-13-2393-2020, publisher: Copernicus GmbH, 2020.

Tokarska, K. B., Gillett, N. P., Arora, V. K., Lee, W. G., and Zickfeld, K.: The influence of non-CO2 forcings on cumulative carbon emissions budgets, Environmental Research Letters, 13, 034 039, https://doi.org/10.1088/1748-9326/aaafdd, publisher: IOP Publishing, 2018.

Tokarska, K. B., Arora, V. K., Gillett, N. P., Lehner, F., Rogelj, J., Schleussner, C.-F., Séférian, R., and Knutti, R.: Uncertainty in carbon budget estimates due to internal climate variability, Environmental Research Letters, 15, 104 064, https://doi.org/10.1088/1748-9326/abaf1b, publisher: IOP Publishing, 2020.

UNFCCC: The Paris Agreement, https://unfccc.int/process-and-meetings/the-paris-agreement, 2015.

Völker, C., Wallace, D. W. R., and Wolf-Gladrow, D. A.: On the role of heat fluxes in the uptake of anthropogenic carbon in the North Atlantic, Global Biogeochemical Cycles, 16, 85–1–85–9, https://doi.org/10.1029/2002GB001897, _eprint: https://onlinelibrary.wiley.com/doi/pdf/10.1029/2002GB001897, 2002.

Watson-Parris, D. and Smith, C. J.: Large uncertainty in future warming due to aerosol forcing, Nature Climate Change, 12, 1111–1113, https://doi.org/10.1038/s41558-022-01516-0, number: 12 Publisher: Nature Publishing Group, 2022.

Williams, R. G., Roussenov, V., Frölicher, T. L., and Goodwin, P.: Drivers of Continued Surface Warming After Cessation of Carbon Emissions, Geophysical Research Letters, 44, 10,633–10,642, https://doi.org/10.1002/2017GL075080, _eprint: https://onlinelibrary.wiley.com/doi/pdf/10.1002/2017GL075080, 2017.

https://doi.org/10.5194/egusphere-2024-488
Preprint. Discussion started: 28 February 2024

Williams, R. G., Ceppi, P., and Katavouta, A.: Controls of the transient climate response to emissions by physical feedbacks, heat uptake and carbon cycling, Environmental Research Letters, 15, 0940c1, https://doi.org/10.1088/1748-9326/ab97c9, publisher: IOP Publishing, 2020.

Williams, R. G., Ceppi, P., Roussenov, V., Katavouta, A., and Meijers, A. J. S.: The role of the Southern Ocean in the global climate response to carbon emissions, Philosophical Transactions of the Royal Society A: Mathematical, Physical and Engineering Sciences, 381, 20220 062, https://doi.org/10.1098/rsta.2022.0062, publisher: Royal Society, 2023.

Zelinka, M. D., Myers, T. A., McCoy, D. T., Po-Chedley, S., Caldwell, P. M., Ceppi, P., Klein, S. A., and Taylor, K. E.: Causes of Higher Climate Sensitivity in CMIP6 Models, Geophysical Research Letters, 47, e2019GL085 782, https://doi.org/10.1029/2019GL085782, _eprint: https://onlinelibrary.wiley.com/doi/pdf/10.1029/2019GL085782, 2020.

Zelinka, M. D., Smith, C. J., Qin, Y., and Taylor, K. E.: Comparison of methods to estimate aerosol effective radiative forcings in climate models, Atmospheric Chemistry and Physics, 23, 8879–8898, https://doi.org/10.5194/acp-23-8879-2023, publisher: Copernicus GmbH, 2023.

Zickfeld, K., Eby, M., Matthews, H. D., and Weaver, A. J.: Setting cumulative emissions targets to reduce the risk of dangerous climate change, Proceedings of the National Academy of Sciences, 106, 16 129–16 134, https://doi.org/10.1073/pnas.0805800106, publisher: Proceedings of the National Academy of Sciences, 2009.

Zickfeld, K., Eby, M., Weaver, A. J., Alexander, K., Crespin, E., Edwards, N. R., Eliseev, A. V., Feulner, G., Fichefet, T., Forest, C. E., Friedlingstein, P., Goosse, H., Holden, P. B., Joos, F., Kawamiya, M., Kicklighter, D., Kienert, H., Matsumoto, K., Mokhov, I. I., Monier, E., Olsen, S. M., Pedersen, J. O. P., Perrette, M., Philippon-Berthier, G., Ridgwell, A., Schlosser, A., Deimling, T. S. V., Shaffer, G., Sokolov, A., Spahni, R., Steinacher, M., Tachiiri, K., Tokos, K. S., Yoshimori, M., Zeng, N., and Zhao, F.: Long-Term Climate Change Commitment and Reversibility: An EMIC Intercomparison, Journal of Climate, 26, 5782–5809, https://doi.org/10.1175/JCLI-D-12-00584.1, publisher: American Meteorological Society Section: Journal of Climate, 2013.

Ziehn, T., Chamberlain, M. A., Law, R. M., Lenton, A., Bodman, R. W., Dix, M., Stevens, L., Wang, Y.-P., and Srbinovsky, J.: The Australian Earth System Model: ACCESS-ESM1.5, Journal of Southern Hemisphere Earth Systems Science, 70, 193–214, https://doi.org/10.1071/ES19035, publisher: CSIRO PUBLISHING, 2020.